Biological Cybernetics (2019) 113:561–577
https://doi.org/10.1007/s00422-019-00809-6

Biological Cybernetics

ORIGINAL ARTICLE

Investigating the role of gap junctions in seizure wave propagation

Laura R. González-Ramírez[1] · **Ava J. Mauro**[2]

Received: 25 June 2019 / Accepted: 13 October 2019 / Published online: 6 November 2019

Abstract
The effect of gap junctions as well as the biological mechanisms behind seizure wave propagation is not completely understood. In this work, we use a simple neural field model to study the possible influence of gap junctions specifically on cortical wave propagation that has been observed in vivo preceding seizure termination. We consider a voltage-based neural field model consisting of an excitatory and an inhibitory population as well as both chemical and gap junction-like synapses. We are able to approximate important properties of cortical wave propagation previously observed in vivo before seizure termination. This model adds support to existing evidence from models and clinical data suggesting a key role of gap junctions in seizure wave propagation. In particular, we found that in this model gap junction-like connectivity determines the propagation of one-bump or two-bump traveling wave solutions with features consistent with the clinical data. For sufficiently increased gap junction connectivity, wave solutions cease to exist. Moreover, gap junction connectivity needs to be sufficiently low or moderate to permit the existence of linearly stable solutions of interest.

Keywords Traveling waves · Seizure termination · Gap Junctions

Mathematics Subject Classification 35C07 · 37N25 · 45K05 · 92C20

1 Introduction

Neural field equations have been used to study spatiotemporal brain phenomena in the form of traveling waves and stationary pulses (Amari 1977; Wilson and Cowan 1972; Bressloff 2012). Applications of neural fields to study brain dynamics include modeling EEG rhythms (Liley et al. 2002; Foster et al. 2011), epileptic seizures (Zhao and Robinson 2015), and geometric visual hallucinations (Ermentrout and Cowan 1979; Bressloff et al. 2001), among many other applications. Traditionally, neural field models consider only chemical synaptic connections (Ermentrout 1998; Coombes et al. 2014; Coombes 2005; Bressloff 2012). However, different studies have also incorporated the effect of gap junctional coupling between pairs of neurons and neuronal networks (Coombes 2008; Kopell and Ermentrout 2004; Chow and Kopell 2000; Ermentrout 2006; Lewis and Rinzel 2003; Kepler et al. 1990; Sherman and Rinzel 1992), and in the continuous limit of an infinite number of neurons (Steyn-Ross et al. 2007; Laing 2015; Elvin 2008).

Gap junctions (also called electrical synapses) are small microdomains that form direct intercellular connections that allow diffusion of ions and small molecules between adjacent cells (Goodenough and Paul 2009). They are constructed of assemblies of channel proteins called connexins arranged around a central pore. Gap junctions allow for electrical and chemical communication between cells, as found in the nervous and cardiovascular systems. There is a diversity of connexins that can lead to different ionic selectivities through the channels (Evans and Martin 2002). It has been found that calcium (Ca^{2+}) can move across the gap junctions (Saez et al. 1989; Fujii et al. 2017; Lacar et al. 2011). At the same time, there is evidence that high levels of calcium can close gap junctions (Rose and Loewenstein 1976). Also, there is numerical evidence linking gap junction distribution to the

Communicated by Benjamin Lindner.

LRGR acknowledges support from SIP-IPN 20195566.

✉ Laura R. González-Ramírez
lrgonzalezr@ipn.mx

[1] Departamento de Formación Básica Disciplinaria, Instituto Politécnico Nacional, Unidad Profesional Interdisciplinaria de Ingeniería Campus Hidalgo, San Agustín Tlaxiaca, Hidalgo, Mexico

[2] Department of Chemistry and Biochemistry, University of Notre Dame, Notre Dame, IN, USA

rate of ion and molecule transport. For example, in Chen and Meng (1995), an estimate was obtained for the efficiency of intercellular transport based on different gap junction distributions in the intercellular membrane. Gap junctions are gated and the flow of molecules can be restricted by voltage and chemical agents. Thus, there is a dynamic component determining gap junction connectivity that is also affected by their distribution. In terms of timescales, there is a noticeable difference between the timescale of action of electrical synapses and of chemical synapses. Chemical synapses have a delay from approximately 1 to 100 ms, whereas electrical synapses act with almost no delay (about 0.2 ms) (Coombes and Zachariou 2009). Therefore, gap junction transmit signals more rapidly than chemical synapses do.

There are different mathematical models that have been established to include gap junctions. In Keener and Sneyd (1998), a model of intercellular calcium wave propagation was established as a reaction–diffusion model. In Bressloff (2016), a model of cells connected via stochastically gated gap junctions was established. This model is based on a one-dimensional system with diffusing molecules with appropriate boundary conditions and gated gap junctions. In Steyn-Ross et al. (2007, 2012), Steyn-Ross et al. developed a mean-field treatment of gap junctions establishing an effect of electrical synapses in the form of diffusion. In Laing (2015), Laing introduced gap junctions to quadratic integrate-and-fire neurons. In the latter three works (Steyn-Ross et al. 2007, 2012; Laing 2015), the modeling of gap junctions is based on the assumption that this type of connection obeys Ohm's Law, and their effect is proportional to the voltage difference of the connected cells.

There is evidence found in the literature about spatiotemporal patterns in the form of waves present during seizure events observed in clinical recordings at microscopic and macroscopic scales. In Perucca et al. (2013), it is mentioned that seizure-like events have distinguishable stages: the beginning of the seizure, followed by epileptiform discharges, then spike and wave events, and seizure termination. In Jirsa et al. (2014), fast discharges and spike and wave events are considered fundamental to understanding brain dynamics during seizure-like events of different species. Martinet et al. (2017) assessed the spatiotemporal voltage dynamics during human seizure, finding evidence of traveling waves of activity propagating at microscopic and macroscopic scales during seizure, with more waves and more consistent source directions being detected at the microscopic spatial scale. The authors estimated the wave velocity with a mean value of 390 mm/s during seizure termination and 660 mm/s during pre-seizure. Evangelista et al. (2015) showed that spike and wave patterns toward seizure termination displayed in the thalamo-cortical connectivity. The seizures that presented these wave patterns also displayed an increase of cortical synchronization with an active effect of thalamic outputs. The authors suggest that this cortical synchronization might help achieve seizure termination. In Proix et al. (2018), a model of seizure dynamics observed in epilepsy was established and compared to clinical data concluding that spike and wave discharges have a part in synchronous seizure termination. Schevon et al. (2012); Weiss et al. (2013) proposed that signature brain dynamics during epilepsy are led by an ictal wavefront that permits the presence of traveling waves of synaptic activity. These waves further induce small-scale slow dynamics that might determine mechanisms of seizure termination (Smith et al. 2016). In general, all the above evidence of spatiotemporal patterns present during seizure events suggests that understanding these kinds of patterns present during epileptic seizures might help improve treatment methods to treat drug-resistant epilepsies.

The effect of gap junctions during epileptic seizures is still unknown. It has been suggested that propagation of activity during epileptic seizures is independent of the effect of gap junctions (Zhang et al. 2014) or that the effect of gap junctions on propagation is not significant (Mylvaganam et al. 2014). In contrast, references Jin and Chen (2011); Carlen et al. (2000); Dudek et al. (1998) reported that gap junctions are of great importance in the generation, synchronization, and development of seizures. Thus, we find contradictory evidence in the literature about the role of electrical synapses during seizures. To address this controversy, we establish a voltage-based neural field model describing the mean activity of an excitatory and an inhibitory population preceding seizure termination to study the possible effect of gap junctions on wave propagation. In this neural field model, we include both chemical and electrical synapses. Our goal is to indirectly attack the possible effect of gap junctions on seizures by studying the effect of gap junctions on wave propagation, which has been observed in vivo before seizure termination (González-Ramírez et al. 2015). In González-Ramírez et al. (2015), a simple activity-based neural field model consisting of a chemically coupled excitatory population as well as an adaptation term was used to model traveling wave solutions observed preceding seizure termination. In the model presented here, we establish a voltage-based neural field consisting of an excitatory population and an inhibitory population as well as both chemical and electrical-like synapses. The addition of more features in the modeling process makes it more feasible to investigate the effect of different factors on the existence of wave solutions observed preceding seizure termination. Thus, we can improve our biological hypothesis in an aim to understand the mechanisms leading to seizure wave propagation.

The paper is structured in the following format. In Sect. 2, we establish the voltage-based mathematical model; we then explore the existence of wave solutions and the effect of parameter choices. In Sect. 3, we study the effect of gap junc-

tions on wave propagation with features consistent with in vivo observations. We first focus on the existence of traveling wave solutions and later discuss the properties of these wave solutions to characterize one-bump or two-bump solutions displaying the properties of interest in this model. In Sect. 4, we perform a linear stability analysis of the one-bump traveling wave solutions and describe the extension to the case of two-bump solutions. In Sect. 5, we perform numerical simulations to validate our theoretical results for one-bump solutions. Finally, we present the conclusions in Sect. 6. The motivation of the model is described in Appendix A.

2 Mathematical model

We consider a voltage-based neural field model consisting of an excitatory and an inhibitory population. We incorporate the effect of electrical synapses through the addition of diffusion terms for both the excitatory and inhibitory populations (Steyn-Ross et al. 2007; Elvin 2008). Additional information about the model motivation is provided in Appendix A.

Let $u_e(x,t)$ and $u_i(x,t)$ be variables describing the local activities of the excitatory and inhibitory populations, respectively. The following equations determine the time evolution of $u_e(x,t)$ and $u_i(x,t)$:

$$\begin{aligned}\frac{\partial u_e}{\partial t}(x,t) =& -\alpha_e u_e(x,t) + \alpha_e g_{ee} \otimes H(u_e(x,t)-k_e) \\ & - \alpha_e g_{ie} \otimes H(u_i(x,t)-k_i) + D_e^2 \frac{\partial^2 u_e}{\partial x^2}(x,t) \\ \frac{\partial u_i}{\partial t}(x,t) =& -\alpha_i u_i(x,t) + \alpha_i g_{ei} \otimes H(u_e(x,t)-k_e) \\ & - \alpha_i g_{ii} \otimes H(u_i(x,t)-k_i) + D_i^2 \frac{\partial^2 u_i}{\partial x^2}(x,t)\end{aligned} \tag{1}$$

The states $u_e(x,t)=0$ and $u_i(x,t)=0$ are considered as resting states. $H(\cdot)$ denotes the Heaviside function. The convolutions and the diffusion terms determine the chemical and electrical spatial synaptic contributions, respectively. The convolutions are defined by

$$g_{jk} \otimes w(x,t) = \frac{1}{2\sigma_{jk}} \int_{-\infty}^{+\infty} e^{-\frac{|x-y|}{\sigma_{jk}}} w(y,t)\,\mathrm{d}y \tag{2}$$

where we chose an exponential function as the kernel of the convolution. A more general function can also be used (Ermentrout 1998).

The parameters of model (1) are defined as follows: α_e and α_i are the decay rate parameters for the mean activities of the excitatory and inhibitory populations, respectively. The parameters σ_{jk}, for $\{j,k\}=\{e,i\}$, account for the spatial decay of the chemical synaptic connectivity within and between the excitatory and inhibitory populations. The parameters k_j, for $j=\{e,i\}$, represent the activity threshold of each population. The parameters D_e and D_i account for the diffusive gap junction-like coupling strength of the excitatory and inhibitory populations, respectively.

2.1 Parameter assumptions

We establish the following assumptions about the parameters. These assumptions are based on information found in the literature as well as simplifying assumptions to make the mathematical analysis manageable.

(i) We focus our analysis on obtaining traveling wave solutions in the parameter ranges of cortical waves observed in vivo preceding seizure termination. We are mainly interested in wave widths varying from approximately 2000–5000 μm and wave speeds varying from approximately 100–500 μm/ms (González-Ramírez et al. 2015). However, we also explore the existence of waves with features in different ranges.

(ii) In González-Ramírez and Kramer (2018), an activity-based neural field model with an excitatory and an inhibitory population was used to describe traveling waves preceding seizure termination. It was found that it was more feasible to obtain traveling wave solutions in the desired ranges when considering inhibition decaying one order of magnitude slower than excitation. Therefore, we focus mainly on $\alpha_i = \frac{\alpha_e}{10}$. However, the effects of gap junctions on the existence of waves are also explored when both excitation and inhibition are decaying at the same rate. The delay of chemical synapses ranges from 1 ms to 100 ms (Coombes and Zachariou 2009), whereas the electrical synapses act with almost no delay. Given the difference between the action timescales of the two types of synapses, it is difficult to establish a value for α_e. Throughout the manuscript we have fixed a value of $\alpha_e = 1$ (1/ms) and we have explored the existence of traveling wave solutions with this timescale. However, in Fig. 6b, we have also explored the existence of traveling wave solutions for faster timescales and its effect on the existence of traveling wave solutions in the range of interest.

(iii) Following our analysis described below of the traveling wave solutions of (1), we set $\sigma_{ee}=\sigma_{ei}$, $\sigma_{ie}=\sigma_{ii}$, and $\sigma_{ee}<\sigma_{ie}$. The choice of these parameters affects the wave profile as shown in Fig. 1. In order to obtain traveling wave solutions with the desired profile, we consider the chemical synaptic connectivity acting locally excitatory and laterally inhibitory. This is also motivated by results described in Ermentrout and Terman (2010), Bressloff (2012) for voltage-based neural fields. We consider chemical synaptic connectivity measures ranging from 40μm to 2 mm, as is reported in

the literature (Reimann et al. 2013; Wilson and Cowan 1972; Peyrache et al. 2012; Braitenberg and Schuz 1998; Frascoli et al. 2011).

(iv) In Fukuda et al. (2006), there are important measurements related to gap junctions that permit the estimation of diffusive strength. In Schmitz et al. (2001), little gap junction connectivity was found between excitatory neurons. This is consistent with theoretical results of Ermentrout (Ermentrout 2006). In Steyn-Ross et al. (2007), a mean-field model was developed including gap junctions obtaining Turing patterns. Using the results found in Fukuda et al. (2006), gap junction connectivity was estimated in Steyn-Ross et al. (2007) under different connectivities obtaining ranges varying from 0.1 to 0.6 cm^2 for the inhibitory population. These results will be analyzed later in the manuscript. In Steyn-Ross et al. (2007), they used the results of Schmitz et al. (2001) and set the excitatory diffusion coefficient to be a fraction of the inhibitory diffusion coefficient. They also explored the possibility of diffusion coefficients closer to being equal, i.e., $D_e = D_i$. Motivated by this, in our work we explore two possibilities: $D_e = \frac{D_i}{10}$ and $D_e = D_i$. We remark that the diffusion coefficients are squared in model (1).

2.1.1 Traveling wave solutions

We are interested in traveling wave solutions of system (1). To obtain these solutions, we rewrite the system in a moving coordinate frame $z = x - ct$, with $c > 0$, and find stationary solutions of this system. The stationary solutions are traveling waves moving to the right with a constant speed c and a constant width w. We are particularly interested in pulse (one-bump) solutions as observed in the clinical data (González-Ramírez et al. 2015). However, two-bump solutions could also model the "reverberation" of activity described in González-Ramírez et al. (2015). Therefore, we assume that the activity threshold that determines the Heaviside function is crossed at least twice each for the excitatory and inhibitory populations, at the points $z = \{w_{e0}, w_{ef}\}$ and $z = \{w_{i0}, w_{if}\}$, respectively. For a right-moving traveling wave, w_{jf} is the right-most point where the solution u_j crosses the threshold k_j, and w_{j0} is the left-most point where u_j crosses k_j, for $j = \{e, i\}$. These assumptions determine conditions for existence of waves and permit the existence of one-bump solutions (which cross the threshold exactly twice) or two-bump solutions (which cross the threshold four times). For the moment, we assume that $w_{i0} \leq w_{e0} \leq w_{if} \leq w_{ef}$. That is, an excitatory wave is followed by an inhibitory wave. In Sect. 2.1.3, we address this assumption and study different scenarios for these four parameters. The width of the excitatory wave is determined by $w_{ef} - w_{e0}$, and the width of the inhibitory wave is determined by $w_{if} - w_{i0}$.

Assuming nonzero diffusion coefficients and using a Green's function (Evans 2010; Stakgold and Holst 2011), we can explicitly obtain excitatory and inhibitory traveling wave solutions of system (1) having the following profile:

$$u_e^\star(z) = \begin{cases} u_{e1} & \text{if } z \leq w_{i0} \\ u_{e2} & \text{if } w_{i0} < z \leq w_{e0} \\ u_{e3} & \text{if } w_{e0} < z \leq w_{if} \\ u_{e4} & \text{if } w_{if} < z \leq w_{ef} \\ u_{e5} & \text{if } z > w_{ef} \end{cases} \tag{3}$$

$$u_i^\star(z) = \begin{cases} u_{i1} & \text{if } z \leq w_{i0} \\ u_{i2} & \text{if } w_{i0} < z \leq w_{e0} \\ u_{i3} & \text{if } w_{e0} < z \leq w_{if} \\ u_{i4} & \text{if } w_{if} < z \leq w_{ef} \\ u_{i5} & \text{if } z > w_{ef} \end{cases} \tag{4}$$

The different terms that form the parts of these solutions and a sketch of their derivation are presented in Appendix B.

2.1.2 Conditions for the existence of traveling wave solutions

The existence of the traveling wave solutions described above is determined by glueing conditions (also called matching conditions), which are conditions on the points where the activity achieves the chemical synaptic threshold:

$$u_e(w_{e0}) = u_e(w_{ef}) = k_e \tag{5}$$

$$u_i(w_{i0}) = u_i(w_{if}) = k_i \tag{6}$$

In order to have a traveling wave solution moving with speed c and width w, Eqs. (5) and (6) need to be satisfied. In Sect. 2.1.5, we explore the existence of such waves with speed and width in the desired range of interest (see Assumption (i) above). Before that, in Sect. 2.1.3, we establish more parameter relationships.

Given the parameter assumptions that we have established above, there are six free parameters remaining: α_e, D_i, σ_{ee}, σ_{ie}, k_e and k_i. We note, however, that k_e and k_i are determined by Eqs. (5) and (6), so we only need to focus on the four parameters α_e, D_i, σ_{ee} and σ_{ie}. Also, we need to further restrict the assumption $w_{i0} \leq w_{e0} \leq w_{if} \leq w_{ef}$ to simplify our problem. To do so, in Sect. 2.1.3, we fix the four free parameters (α_e, D_i, σ_{ee} and σ_{ie}) and explore the effect of changing the terms w_{e0}, w_{i0}, w_{ef} and w_{if} restricted to satisfy (5) and (6). In particular, in the next two subsections we see the effect of changing the assumption that $w_{i0} \leq w_{e0} \leq w_{if} \leq w_{ef}$ on the traveling wave profile, motivating further parameter assumptions. With this, we aim to restrict the relationship between the w_j terms to further

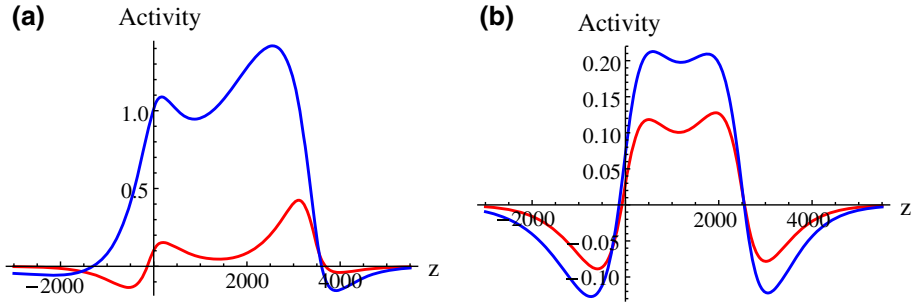

Fig. 1 Traveling wave profile. Examples of traveling wave profiles of the excitatory (red) and inhibitory (blue) populations. **a** Two-bump solution. This two-bump solution will be addressed in Sect. 3. **b** Pulse solution. The parameters used in each subplot are the following: **a** $\alpha_e = 1\ 1/\text{ms}, \alpha_i = 0.1\ 1/\text{ms}, D_e = 10\,\mu\text{m}/\sqrt{\text{ms}}, D_i = 100\,\mu\text{m}/\sqrt{\text{ms}}, \sigma_{ej} = 200\,\mu\text{m}, \sigma_{ij} = 500\,\mu\text{m}$ for $j = \{e, i\}$; **b** $\alpha_e = 1\ 1/\text{ms}, \alpha_i = 0.1\ 1/\text{ms}, D_e = 300\,\mu\text{m}/\sqrt{\text{ms}}, D_i = 300\,\mu\text{m}/\sqrt{\text{ms}}, \sigma_{ej} = 200\,\mu\text{m}, \sigma_{ij} = 500\,\mu\text{m}$ for $j = \{e, i\}$ (color figure online)

explore the parameter relationship between α_e, D_i, σ_{ee} and σ_{ie}.

2.1.3 Traveling wave profile

In contrast with activity-based neural fields (Bressloff 2012; Ermentrout 1998), in the voltage-based neural field formulation the traveling wave solution profile is more strongly affected by changing the parameters. The kernel of the connectivity term, and therefore the extent of the synaptic connectivity, as well as the gap junctions are important factors in the wave profile (see Fig. 1).

We have four free parameters concerning the width of the traveling wave: w_{e0}, w_{i0}, w_{ef}, and w_{if}. These parameters determine the start and the end of the traveling wave profile for the excitatory and inhibitory populations. Since we are considering a right-moving traveling wave solution (i.e., $z = x - ct$), we are assuming that an initial excitatory wave (that starts to propagate at w_{ef}) produces an inhibitory wave (at w_{if}). Inhibition induces the excitatory activity to go back toward rest (at w_{e0}), which then induces the inhibitory activity to go back toward the rest state (at w_{i0}). After analyzing wave solution profiles under different conditions for w_{e0} and w_{i0} satisfying $w_{i0} \leq w_{e0}$, we do not find a significant effect on the profile of the wave under these variations. Therefore, given that the wave solutions are translationally invariant and to simplify the number of free parameters, we assume that the excitatory and inhibitory waves start to go back to the rest state at the same point, that is $w_{e0} = w_{i0} = 0$. Two free parameters remain concerning the width of the traveling wave solutions: w_{ef} and w_{if}. After numerical examination under different parameter configurations, we find that the choice of w_{ef} and w_{if} has a significant effect on the traveling wave profile. Therefore, we set $w_{if} = w_{ef} - \Delta w$ for $\Delta w \geq 0$ and study the effect of changing Δw in the existence conditions determined by (5) and (6). That is, we are assuming that the excitatory and inhibitory waves do not start to propagate at the same time (excitatory wave starts at w_{ef} and inhibitory wave starts at w_{if}), but both populations go below their respective thresholds at the same time (at $w_{i0} = w_{e0}$). For now, we focus only on the existence of traveling wave solutions and later discuss whether they are one-bump or multi-bump solutions.

2.1.4 Determining Δw

We analyze different parameter choices to explore the effect of Δw on the existence of traveling wave solutions that satisfy Eqs. (5) and (6). For small values of Δw, we find the existence of two traveling wave solutions, whose speed and width do not lie in the range of interest from Assumption (i). After a critical value that depends on the other parameters used, a new traveling wave solution appears (see Fig. 2). This wave solution has speed and width in the desired range of interest. We find that small changes to the parameters produce qualitatively similar results. However, the critical value of Δw is determined by the different choices of parameters. In particular, giving a choice of parameter values a high enough value of D_i destroys the upper branch of physically realistic wave solutions. This will be further discussed in Sect. 3. Due to the numerical examination in Fig. 2 and our choice of parameters, for the moment we fix $\Delta w = 400$ to be in the range of parameters of observable waves. However, in Fig. 5, we explore the influence of gap junctions on the existence of traveling wave solutions under different scenarios for Δw to determine wave propagation.

2.1.5 Existence of traveling wave solutions

We determine the existence of traveling wave solutions that satisfy (5) and (6). In the figures, we plot the excitatory wave width, w_{ef}. The inhibitory wave width is determined from the assumption $w_{if} = w_{ef} - \Delta w$. Considering both Eqs. (5) and (6) to be satisfied, we obtain Fig. 3. In Fig. 3a, we have curves determining conditions (5) and (6) for the excitatory (red) and inhibitory (blue) populations, respectively. The points

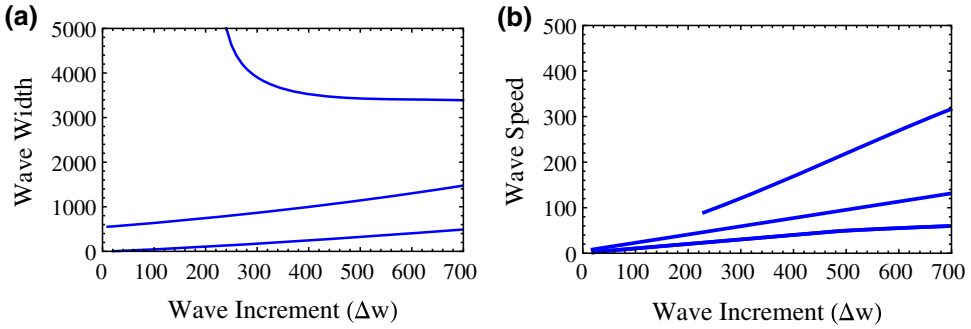

Fig. 2 Existence of traveling wave solutions determined by Δw. **a** Wave width (μm) versus wave increment (Δw). For low values of Δw, we observe the existence of two traveling wave solutions. The width of these waves is below 800 μm, which is well below the range of interest (see Assumption (i)). Above a critical value of $\Delta w \approx 225\mu$m, a new traveling wave solution appears whose wave width lies between 3000 μm and 5000 μm, which is a subset of the range of interest. **b** Wave speed (μm/ms) versus wave increment (Δw). Similarly to **a**, for low values of Δw, we observe the existence of two traveling wave solutions whose speed lies below the range of interest (below 100 μm/ms). Above the same critical value as in **a**, we see the existence of a faster wave solution whose speed lies between 100 μm/ms and 350 μm/ms, which is within the range of interest. In **a**, **b**, we show the existence of traveling wave solutions for the given parameter configuration. Not all the solutions lie in the range of interest. We note that for small values of Δw, two low branches of wave solutions exist giving unrealistic wave features. For a value of $\Delta w \approx 225\mu$m, a new branch of traveling wave solutions appears with features more consistent with the in vivo data. We also note that as Δw is increased, the width and speed of the wave solutions in the middle branch increase toward the range of interest. Parameters used for this figure: $\alpha_e = 1$ 1/ms, $\alpha_i = 0.1$ 1/ms, $\sigma_{ej} = 200\,\mu$m and $\sigma_{ij} = 500\,\mu$m for $j = \{e, i\}$, $D_i = 100\,\mu\text{m}/\sqrt{\text{ms}}$, $D_e = 10\,\mu\text{m}/\sqrt{\text{ms}}$. Small changes in parameters produce qualitatively similar results and produce a variation of the critical value of Δw

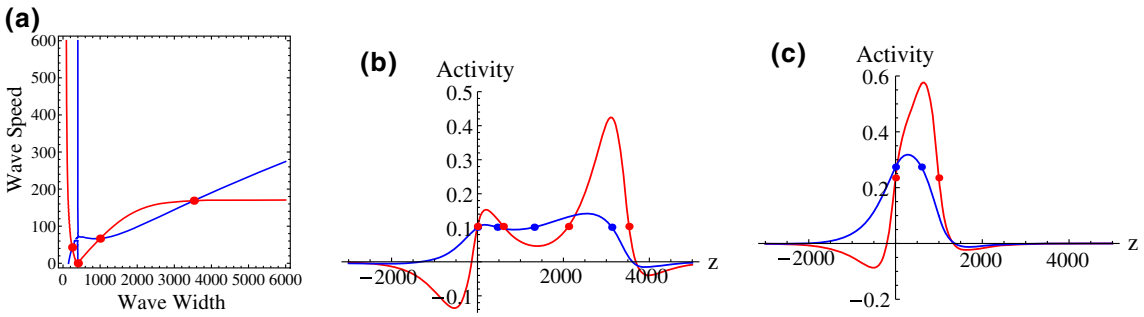

Fig. 3 Existence of traveling wave solutions. **a** Existence of wave solutions is determined by the intersection (red points) of conditions (5) (red curve) and (6) (blue curve). We observe the existence of two traveling wave solutions whose wave width is below 400 μm and are not in the range of interest. There are also two wave solutions lying in or very close to the range of interest. One of these waves has a wave width of approximately 3525 μm and a wave speed of approximately 168 μm/ms, which is within the range of interest (wave profile shown in **b**). The other wave solution of interest has a wave width of approximately 997 μm and a wave speed of approximately 66 μm/ms, which lies very close to the range of interest (wave profile shown in **c**). **b, c** Traveling wave solution for the excitatory population (red) and the inhibitory population (blue). The red and blue points indicate where the activity threshold is achieved for the excitatory and inhibitory population, respectively. The traveling wave solution in **b** is a two-bump solution that crosses the activity threshold four times. The traveling wave solution in **c** is a pulse (one-bump) solution that crosses the activity threshold exactly two times. Parameters used for this figure: $\alpha_e = 1$ 1/ms, $\alpha_i = 0.1$ 1/ms, $\sigma_{ej} = 200\,\mu$m and $\sigma_{ij} = 500\,\mu$m for $j = \{e, i\}$, $D_i = 100\,\mu\text{m}/\sqrt{\text{ms}}$, $D_e = 10\,\mu\text{m}/\sqrt{\text{ms}}$ (color figure online)

of intersection of the two curves determine traveling wave solutions that satisfy both conditions. In the example shown in Fig. 3, we observe the existence of four different traveling wave solutions. Two of these solutions have widths and speeds below the range of interest as well as physically unrealistic widths given the assumption $w_{if} = w_{ef} - \Delta w$. The two wave solutions in the range of interest are further considered. It is important to remark that these results are obtained for a fixed value of D_i and a fixed value of Δw.

In the following section, we explore the existence of wave solutions varying the diffusive coupling strength. Also, in Sect. 4, we explore the linear stability of solutions of interest. It is important to determine the stability of the traveling wave solutions obtained because we are interested in traveling wave propagation observed in vivo; a traveling wave solution that is observable in vivo would be expected to be stable. In this work, we will focus only on the linear stability of pulse solutions.

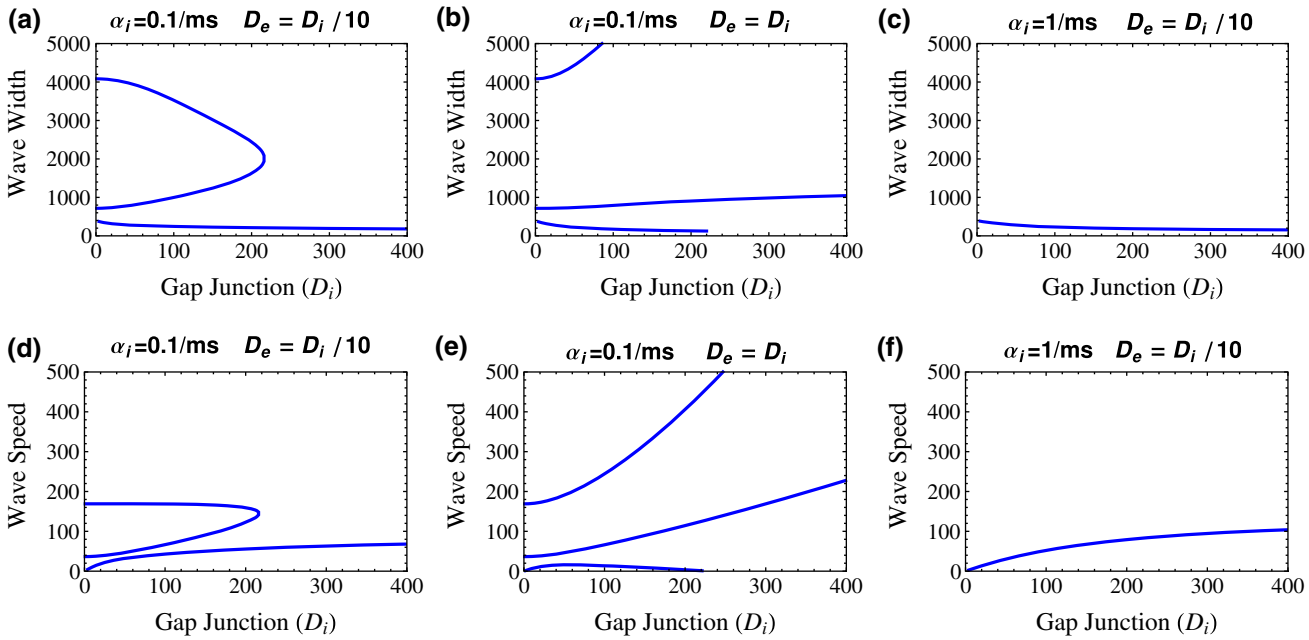

Fig. 4 Effect of gap junctions on wave propagation. We describe the exact conditions regarding the gap junction coupling coefficient (D_i) for wave propagation in the range of interest. First row **a**–**c** shows excitatory wave width w_{ef} (μm) versus diffusive coupling coefficient D_i (μm/$\sqrt{\text{ms}}$). Second row **d**–**f** shows wave speed c (μm/ms) versus diffusive coupling coefficient D_i. **a, d** We note the existence of three branches of traveling wave solutions. The upper branch lies in the range of interest and consists of mostly two-bump traveling wave solutions and unstable one-bump solutions. The upper branches exist up to a critical value of D_i near 220 μm/$\sqrt{\text{ms}}$. The upper branches lie in the range of interest, and linear stability analysis suggests that the middle branch is stable for D_i less than approximately 140 μm/$\sqrt{\text{ms}}$ (see Sect. 4). The lower branch is not in the range of interest and is not physically realistic as it has a width smaller than 400 μm and we are under the assumption $w_{if} = w_{ef} - 400$. We also note that the gap junction connectivity established in Assumption iv, where Turing patterns occur, lies well above the critical value of D_i. **b, e** We note the existence of an upper branch of traveling wave solutions up to a critical value of D_i. We also note that the middle branch does not lie in the range of interest and the lower branch cannot satisfy the assumption $w_{if} = w_{ef} - 400$. **c, f** We note the existence of a low branch whose width and speed do not lie in the range of interest. Parameters fixed in all subplots: $\alpha_e = 1$ 1/ms, σ_{ej} = 200 μm and σ_{ij} = 500 μm for $j = \{e, i\}$, $\Delta w = 400$. Parameters used in **a** and **d**: $\alpha_i = 0.1$ 1/ms, $D_e = \frac{D_i}{10}$. Parameters used in **b**, **e**: $\alpha_i = 0.1$ 1/ms, $D_e = D_i$. Parameters used in **c** and **f**: $\alpha_i = 1$ 1/ms and $D_e = \frac{D_i}{10}$. We have extensively explored different parameter configurations and obtain qualitatively consistent results after a small variation in parameters. In particular, the parameters used in plots **a**, **d** show one of the best scenarios in which the middle and upper branches of traveling wave solutions lie in or very close to the range of interest

3 Effect of gap junctions on cortical wave propagation

In this section, we analyze the effect of gap junctions on the existence of cortical traveling wave solutions. To do so, we fix the parameters α_e, σ_{ej}, and σ_{ij} subject to the parameter assumptions established above. We then vary the parameters D_e and D_i subject to the parameter relationship (iv) and use Eqs. (5) and (6) to determine the existence of traveling wave solutions. In Figs. 4 and 5, we explore the effect of gap junction connectivity on the existence of traveling wave solutions. In Fig. 7, we describe the properties of traveling wave solutions shown in Fig. 4a and label them as two-bump traveling wave solutions or one-bump traveling wave solutions. In Fig. 7, we also establish the linear stability of one-bump traveling wave solutions by means of an Evans function developed in Sect. 4. In this way, we determine the conditions due to the gap junctions for wave propagation in the range of interest. After carefully analyzing distinct parameter configurations (see Fig. 4), we conclude the importance of gap junctions on wave propagation. In particular, for low values of inhibitory diffusive coupling strength and slow-decaying inhibition (i.e., $\alpha_i = \alpha_e/10$), we show the existence of three traveling wave solutions for the excitatory population with different speeds and widths (Fig. 4a, b, d, e). Of these wave solutions, the one with the narrowest width and slowest speed is not in the range of interest; additionally, its width lies below 400 μm and we are considering $w_{if} = w_{ef} - \Delta w$ with $\Delta w = 400$, so we do not obtain a physically feasible traveling wave solution for the inhibitory population. The two remaining traveling wave solutions have widths and speeds that lie in or near the range of interest. In Fig. 4a, d, after we increase diffusive coupling strength enough, we see a bifurcation of the two significant solutions collapsing and disappearing. Hence, for sufficiently large values of D_i, only the non-realistic traveling wave solution is present. Lin-

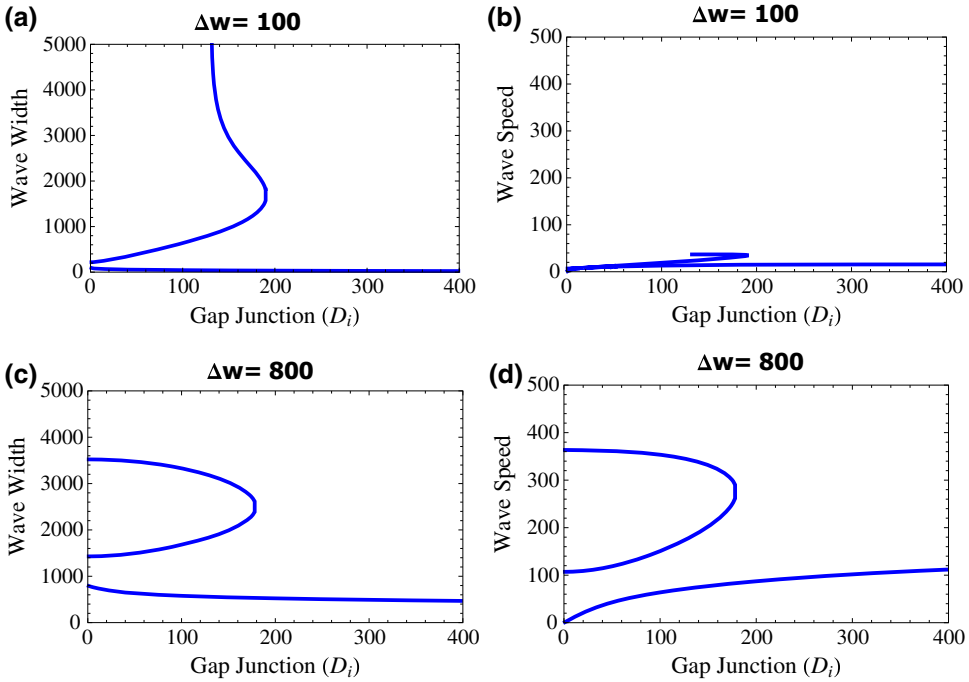

Fig. 5 Effect of gap junctions on wave propagation modifying Δw. We now consider different choices for Δw and study the effect of gap junctions on seizure wave propagation. First row **a, b** shows wave width and wave speed versus diffusive coupling coefficient D_i, with $\Delta w = 100\mu$m. In **a**, we observe wave solutions whose width lies in the range of interest. In **b**, we observe the appearance of a new solution at $D_i \approx 130\,\mu\text{m}/\sqrt{\text{ms}}$ due to the fact that both matching conditions have asymptotes at $w_{ef} \approx 30\,\mu m$ for that value of D_i (not shown). However, all the wave solutions in **b** are not in the range of interest. This analysis is consistent with Fig. 2. Second row **c, d** shows wave width and wave speed versus diffusive coupling coefficient D_i for a choice of $\Delta w = 800\mu$m. In **c, d**, we observe wave solutions whose speed and width lies in the range of interest. However, $\Delta w = 800\mu$m implies a large lag between the excitatory wave solution and the inhibitory wave solution. In **a**–**d**, we obtain qualitatively similar results as in Fig. 4a, d, implying a critical value of D_i above which no traveling wave solutions exist in the range of interest. Parameters fixed in all subplots: $\alpha_e = 1$ 1/ms, $\alpha_i = 0.1$ 1/ms, $\sigma_{ej} = 200\,\mu$m and $\sigma_{ij} = 500\,\mu$m for $j = \{e, i\}$, $D_e = \frac{D_i}{10}$

ear stability analysis developed in Sect. 4 suggests that the one-bump solutions in the middle branch are stable up to some value of D_i before the bifurcation value (Fig. 7a). The exact value at which they change stability is determined by the parameter configuration. After this value and up to the bifurcation value of D_i, one-bump solutions in the middle branch are unstable. In the upper branch, we initially have two-bump traveling wave solutions that transform into unstable one-bump traveling wave solutions before the bifurcation value that destroys the middle and upper branches. For more details, see Fig. 7. Thus, in order to have traveling wave solutions as observed in the in vivo clinical data, gap junctions play an important role as the diffusive strength needs to be sufficiently low or moderate to permit the presence of (linearly) stable traveling waves. In Fig. 4a, d, we note that the critical value of D_i that determines the bifurcation is well below the values established in Assumption iv in which Turing patterns occur. Therefore, traveling wave solutions exist in this model in ranges of feasible gap junction connectivities. In Fig. 4c, f, we explore the same scenario for a faster-acting inhibition (i.e., $\alpha_i = \alpha_e$) and obtain no wave solutions in the range of interest. This is consistent with analysis developed in González-Ramírez and Kramer (2018).

In Fig. 5, we perform a similar analysis changing the choice of Δw. We obtain results that are consistent with the results in Fig. 2. For small values of Δw, we do not find wave solutions of interest. For values of Δw greater than a critical value, we obtain wave solutions lying in the range of interest. However, biophysical mechanisms cannot permit a very large value of Δw. Also, as far as we know, it is not possible to estimate the in vivo value of Δw.

In Fig. 6a, we analyze the effect of modifying the choice of Δw on the existence of traveling wave solutions. In particular, we show the minimum and maximum gap coefficient (D_i) such that the traveling wave solution is in the range of interest. Also, in Fig. 6b, we analyze the effect of changing the timescale of the excitatory population (α_e) on the existence of traveling wave solutions. We find that the existence of traveling wave solutions is affected by both the diffusion coefficient D_i and α_e.

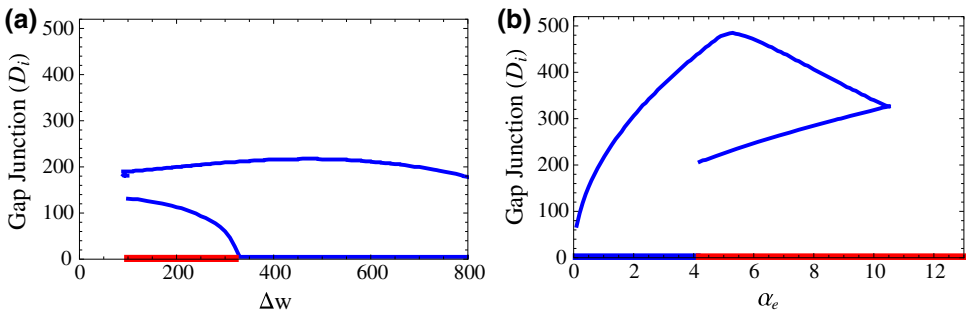

Fig. 6 Maximum and minimum D_i that determine the existence of traveling wave solutions. **a** The plot shows the range of values of D_i that determines the existence of traveling wave solutions for a given Δw. The red line indicates the minimum value of D_i that determines traveling wave solutions whose width are below the range of interest. The blue lines indicate the minimum and maximum values of D_i that determine the existence of traveling wave solutions in the range of interest (between 1000 μm to 6000 μm). We note that regardless of our choice of Δw, the maximum diffusion coefficient D_i is less than 250. This indicates that for all choices of Δw, the bifurcation shown in Figs. 4 and 5 is always present. **b** Similarly to **a**, we now explore the existence of traveling wave solutions for different timescales of the excitatory population (assuming $\alpha_i = \alpha_e/10$). For α_e less than approximately 4, we see that the minimum and maximum values of D_i range from 1 to approximately 400. For α_e values larger than 4, we see a bifurcation in the way the diffusion coefficient affects the existence of traveling wave solutions. That is, low values of D_i give rise to unrealistic traveling wave solutions. The diffusion coefficient that permits the existence of traveling wave solutions is more limited as α_e increases. Finally, for values of α_e greater than 11, we only obtain non-realistic traveling wave solutions. Parameters fixed in all subplots: $\alpha_i = \alpha_e/10$, $\sigma_{ej} = 200$ μm and $\sigma_{ij} = 500$ μm for $j = \{e, i\}$, $D_e = \frac{D_i}{10}$. Parameters used in **a** $\alpha_e = 1$ 1/ms. Parameters used in **b** $\Delta w = 400$ (color figure online)

4 Stability analysis

We are interested in the stability analysis of the traveling wave solutions determined above (see Fig. 4) as we wish to relate these solutions to clinical data observed in vivo. In order to do so, we focus our analysis on the linear stability of these solutions as linear stability suggests important features of the traveling wave solutions. To determine the linear stability analysis, we first bound the essential spectrum on the left-hand complex plane and determine an Evans function on a convenient domain whose zeros determine the point eigenvalues of the system. For this, we follow the work developed for nonlocal equations in Kapitula et al. (2004) and Sandstede (2007).

In this work, we only focus on the construction of an Evans function for one-bump traveling wave solutions where the activity threshold is crossed at exactly two points. It is also mentioned how to incorporate a similar analysis for two-bump wave solutions.

We consider system (1) under the moving frame (z, t) where we consider the variable $z = x - ct$ and formally linearize system (1) about the traveling wave solutions $u_e^\star$ and $u_i^\star$ (determined by (3) and (4)). For this, we consider perturbations $u_e(z,t) = u_e^\star(z) + \bar{u}_e(z,t)$ and $u_i(z,t) = u_i^\star(z) + \bar{u}_i(z,t)$ where $\bar{u}_e(z,t)$ and $\bar{u}_i(z,t)$ are small. When linearizing, we consider the Heaviside function as a distribution and use properties of the convolution term. After linearizing we obtain:

$$
\begin{aligned}
&\frac{\partial \bar{u}_e}{\partial t}(z,t) - c\frac{\partial \bar{u}_e}{\partial z}(z,t) \\
&\quad = -\alpha_e \bar{u}_e(z,t) \\
&\qquad + \alpha_e \int_{-\infty}^{\infty} g_{ee}(z-y)\delta(u_e^\star(y) - k_e)\bar{u}_e(y,t)\mathrm{d}y \\
&\qquad - \alpha_e \int_{-\infty}^{\infty} g_{ie}(z-y)\delta(u_i^\star(y) - k_i)\bar{u}_i(y,t)\mathrm{d}y \\
&\qquad + D_e^2 \frac{\partial^2 \bar{u}_e}{\partial t^2}(z,t) \\
&\frac{\partial \bar{u}_i}{\partial t}(z,t) - c\frac{\partial \bar{u}_i}{\partial z}(z,t) \\
&\quad = -\alpha_i \bar{u}_i(z,t) \\
&\qquad + \alpha_i \int_{-\infty}^{\infty} g_{ei}(z-y)\delta(u_e^\star(y) - k_e)\bar{u}_e(y,t)\mathrm{d}y \\
&\qquad - \alpha_i \int_{-\infty}^{\infty} g_{ii}(z-y)\delta(u_i^\star(y) - k_i)\bar{u}_i(y,t)\mathrm{d}y \\
&\qquad + D_i^2 \frac{\partial^2 \bar{u}_i}{\partial t^2}(z,t)
\end{aligned}
\tag{7}
$$

Assuming separation of variables, we propose that $\bar{u}_e(z,t) = \mathrm{e}^{\lambda t}\bar{u}_e(z)$ and $\bar{u}_i(z,t) = \mathrm{e}^{\lambda t}\bar{u}_i(z)$ where $\lambda \in \mathbb{C}$. This assumption will establish the eigenvalue problem. Determining the values of λ for which bounded solutions of this eigenvalue problem exist will help determine the linear stability of the traveling wave solutions (for details see Sandstede 2002). After substituting the assumption, we obtain a sys-

tem of ordinary differential equations where the derivative is taken with respect to z. For simplicity and to clarify notation, we will remove the bars ($\bar{u}_e(z) = u_e(z)$ and $\bar{u}_i(z) = u_i(z)$).

$$\begin{aligned}\lambda u_e &= cu_e' - \alpha_e u_e + \alpha_e \int_{-\infty}^{\infty} g_{ee}(z-y)\delta(u_e^\star(y) - k_e)u_e(y)\mathrm{d}y \\ &\quad - \alpha_e \int_{-\infty}^{\infty} g_{ie}(z-y)\delta(u_i^\star(y) - k_i)u_i(y)\mathrm{d}y + D_e^2 u_e'' \\ \lambda u_i &= cu_i' - \alpha_i u_i + \alpha_i \int_{-\infty}^{\infty} g_{ei}(z-y)\delta(u_e^\star(y) - k_e)u_e(y)\mathrm{d}y \\ &\quad - \alpha_i \int_{-\infty}^{\infty} g_{ii}(z-y)\delta(u_i^\star(y) - k_i)u_i(y)\mathrm{d}y + D_i^2 u_i''\end{aligned} \tag{8}$$

where the derivatives have been taken with respect to the variable z. We assume that the wave solutions crossed the threshold twice for each the excitatory and the inhibitory population at $\{w_{e0} = 0, w_{ef}\}$ and $\{w_{i0} = 0, w_{if}\}$, respectively. For a two-bump traveling wave solution, we would need to consider for each population the four points at which the activity crosses the threshold. In the case of a pulse solution under the previous assumptions, we obtain:

$$\begin{aligned}\lambda u_e =& cu_e' - \alpha_e u_e + D_e^2 u_e'' \\ &+ \frac{\alpha_e g_{ee}(z)}{\mid u_e^\star(0) \mid} u_e(0) + \frac{\alpha_e g_{ee}(z-w_{ef})}{\mid u_e^\star(w_{ef}) \mid} u_e(w_{ef}) \\ &+ \frac{\alpha_e g_{ie}(z)}{\mid u_i^\star(0) \mid} u_i(0) + \frac{\alpha_e g_{ie}(z-w_{if})}{\mid u_i^\star(w_{if}) \mid} u_i(w_{if}) \\ \lambda u_i =& cu_i' - \alpha_i u_i + D_i^2 u_i'' \\ &+ \frac{\alpha_i g_{ei}(z)}{\mid u_e^\star(0) \mid} u_e(0) + \frac{\alpha_i g_{ei}(z-w_{ef})}{\mid u_e^\star(w_{ef}) \mid} u_e(w_{ef}) \\ &+ \frac{\alpha_i g_{ii}(z)}{\mid u_i^\star(0) \mid} u_i(0) + \frac{\alpha_i g_{ii}(z-w_{if})}{\mid u_i^\star(w_{if}) \mid} u_i(w_{if})\end{aligned} \tag{9}$$

Hence, we deal with a nonlocal eigenvalue problem. We consider a family of bounded linear operators $T(\lambda) : C^2(R, C^2) \to C^0(R, C^2)$ defined by $f(z) \to Df_{zz} + cf_z + (A(\lambda)I)f - K(f(z))$, where $K(f(z))$ is the nonlocal part given by $K(f(z)) = \sum_{j=1}^{m} g(z - z_j) f(z_j)$ for some $g \in C^0$ and $A(\lambda) \in C^{2\times 2}$. Then, clearly system (9) can be rewritten in this form. Also, we note that the nonlocal part of T factors through the space C^m and is compact. On the other hand, we consider the local part of T as $T_{\mathrm{loc}} = D\frac{d^2}{dz^2} + c\frac{d}{dz} + A(\lambda)$. The operators T and T_{loc} differ by a compact operator implying that their essential spectrum is the same (Kapitula et al. 2004). We can compute the essential spectrum of the corresponding T_{loc} determined by (9) by Fourier transforming the system. We obtain that the essential spectrum is determined by the vertical lines $Re(\lambda) = -D_e^2 k^2 - \alpha_e$ and $Re(\lambda) = -D_i^2 k^2 - \alpha_i$ for $k \in R$. In this way, we bound the essential spectrum of the operator T in the left half complex plane. Thus, in order to establish the linear stability of the traveling wave solutions, it is necessary to determine the point eigenvalues.

4.1 Construction of an Evans function

We construct an Evans function for λ in the region $\Omega = \{\lambda \in C \mid Re(\lambda) > -\epsilon\}$ where $\epsilon > 0$, such that the eigenvalues of the corresponding $A(\lambda)$ determined by system (9) have strictly negative real part. Thus, we expect to detect potential wave instabilities in the region Ω. We establish a complex valued Evans function such that the roots of the Evans function are in correspondence with the point eigenvalues. To do so, we start by considering bounded solutions of system (9). Using the variation of parameters formula we obtain:

$$\begin{aligned}u_e(z) =& \frac{\alpha_e}{\sqrt{c^2 + 4D_e^2(\alpha_e + \lambda)}} \\ &\times \Bigg[\int_z^{\infty} \mathrm{e}^{\lambda_1(z-y)} \left(\frac{g_{ee}(y)}{h_e(0)} u_e(0) + \frac{g_{ee}(y-w_{ef})}{h_e(w_{ef})} u_e(w_{ef}) \right. \\ &\left. - \frac{g_{ie}(y)}{h_i(0)} u_i(0) - \frac{g_{ie}(y-w_{if})}{h_i(w_{if})} u_i(w_{if}) \right) \mathrm{d}y \\ &+ \int_{-\infty}^{z} \mathrm{e}^{\lambda_2(z-y)} \left(\frac{g_{ee}(y)}{h_e(0)} u_e(0) + \frac{g_{ee}(y-w_{ef})}{h_e(w_{ef})} u_e(w_{ef}) \right. \\ &\left. - \frac{g_{ie}(y)}{h_i(0)} u_i(0) - \frac{g_{ie}(y-w_{if})}{h_i(w_{if})} u_i(w_{if}) \right) \mathrm{d}y \Bigg]\end{aligned} \tag{10}$$

where $\lambda_1 = \frac{c + \sqrt{c^2 + 4D_e^2(\alpha_e + \lambda)}}{2D_e^2}$, $\lambda_2 = \frac{c - \sqrt{c^2 - 4D_e^2(\alpha_e + \lambda)}}{2D_e^2}$ and $h_e(z) = \mid u_e^\star(z) \mid$ and similarly for the inhibitory population:

$$\begin{aligned}u_i(z) =& \frac{\alpha_i}{\sqrt{c^2 + 4D_i^2(\alpha_i + \lambda)}} \\ &\times \Bigg[\int_z^{\infty} \mathrm{e}^{\lambda_3(z-y)} \left(\frac{g_{ei}(y)}{h_e(0)} u_e(0) + \frac{g_{ei}(y-w_{ef})}{h_e(w_{ef})} u_e(w_{ef}) \right. \\ &\left. - \frac{g_{ii}(y)}{h_i(0)} u_i(0) - \frac{g_{ii}(y-w_{if})}{h_i(w_{if})} u_i(w_{if}) \right) \mathrm{d}y \\ &+ \int_{-\infty}^{z} \mathrm{e}^{\lambda_4(z-y)} \left(\frac{g_{ei}(y)}{h_e(0)} u_e(0) + \frac{g_{ei}(y-w_{ef})}{h_e(w_{ef})} u_e(w_{ef}) \right. \\ &\left. - \frac{g_{ii}(y)}{h_i(0)} u_i(0) - \frac{g_{ii}(y-w_{if})}{h_i(w_{if})} u_i(w_{if}) \right) \mathrm{d}y \Bigg]\end{aligned} \tag{11}$$

where $\lambda_3 = \frac{c + \sqrt{c^2 + 4D_i^2(\alpha_i + \lambda)}}{2D_i^2}$, $\lambda_4 = \frac{c - \sqrt{c^2 - 4D_i^2(\alpha_i + \lambda)}}{2D_i^2}$ and $h_i(z) = \mid u_i^\star(z) \mid$.

We look for the bounded nontrivial solutions of $u_e(z)$ and $u_i(z)$. To do so, we substitute the values of $z = 0$, $z = w_{ef}$ and $z = w_{if}$ in (10) and (11) and rewrite the corresponding system in matrix form taking advantage of the nonlocal terms determining a matrix $D(\lambda)$. By construction, the eigenvalue equation (9) has a nontrivial solution when the determinant of the Evans function vanishes, where

$$E(\lambda) = det\,[D(\lambda) - I] \tag{12}$$

where

$$D(\lambda) = \left(p_1(\lambda)\ p_2(\lambda)\ p_3(\lambda)\ 0_{6\times 1}\ 0_{6\times 1}\ p_6(\lambda) \right)$$

and

$$p_1(\lambda) = \begin{pmatrix} \frac{A_e}{h_e(0)} \left(\int_0^\infty \mathrm{e}^{\lambda_1(-y)} g_{ee}(y)\mathrm{d}y + \int_{-\infty}^0 \mathrm{e}^{\lambda_2(-y)} g_{ee}(y)\mathrm{d}y \right) \\ \frac{A_i}{h_e(0)} \left(\int_0^\infty \mathrm{e}^{\lambda_3(-y)} g_{ei}(y)\mathrm{d}y + \int_{-\infty}^0 \mathrm{e}^{\lambda_4(-y)} g_{ei}(y)\mathrm{d}y \right) \\ \frac{A_e}{h_e(0)} \left(\int_{wef}^\infty \mathrm{e}^{\lambda_1(w_{ef}-y)} g_{ee}(y)\mathrm{d}y + \int_{-\infty}^{w_{ef}} \mathrm{e}^{\lambda_2(w_{ef}-y)} g_{ee}(y)\mathrm{d}y \right) \\ \frac{A_i}{h_e(0)} \left(\int_{wef}^\infty \mathrm{e}^{\lambda_3(w_{ef}-y)} g_{ei}(y)\mathrm{d}y + \int_{-\infty}^{w_{ef}} \mathrm{e}^{\lambda_4(w_{ef}-y)} g_{ei}(y)\mathrm{d}y \right) \\ \frac{A_e}{h_e(0)} \left(\int_{w_{if}}^\infty \mathrm{e}^{\lambda_1(w_{if}-y)} g_{ee}(y)\mathrm{d}y + \int_{-\infty}^{w_{if}} \mathrm{e}^{\lambda_2(w_{if}-y)} g_{ee}(y)\mathrm{d}y \right) \\ \frac{A_i}{h_e(0)} \left(\int_{w_{if}}^\infty \mathrm{e}^{\lambda_3(w_{if}-y)} g_{ei}(y)\mathrm{d}y + \int_{-\infty}^{w_{if}} \mathrm{e}^{\lambda_4(w_{if}-y)} g_{ei}(y)\mathrm{d}y \right) \end{pmatrix} \tag{13}$$

$$p_2(\lambda) = \begin{pmatrix} \frac{-A_e}{h_i(0)} \left(\int_0^\infty \mathrm{e}^{\lambda_1(-y)} g_{ie}(y)\mathrm{d}y + \int_{-\infty}^0 \mathrm{e}^{\lambda_2(-y)} g_{ie}(y)\mathrm{d}y \right) \\ \frac{-A_i}{h_i(0)} \left(\int_0^\infty \mathrm{e}^{\lambda_3(-y)} g_{ii}(y)\mathrm{d}y + \int_{-\infty}^0 \mathrm{e}^{\lambda_4(-y)} g_{ii}(y)\mathrm{d}y \right) \\ \frac{-A_e}{h_i(0)} \left(\int_{wef}^\infty \mathrm{e}^{\lambda_1(w_{ef}-y)} g_{ie}(y)\mathrm{d}y + \int_{-\infty}^{w_{ef}} \mathrm{e}^{\lambda_2(w_{ef}-y)} g_{ie}(y)\mathrm{d}y \right) \\ \frac{-A_i}{h_i(0)} \left(\int_{wef}^\infty \mathrm{e}^{\lambda_3(w_{ef}-y)} g_{ii}(y)\mathrm{d}y + \int_{-\infty}^{w_{ef}} \mathrm{e}^{\lambda_4(w_{ef}-y)} g_{ii}(y)\mathrm{d}y \right) \\ \frac{-A_e}{h_i(0)} \left(\int_{w_{if}}^\infty \mathrm{e}^{\lambda_1(w_{if}-y)} g_{ie}(y)\mathrm{d}y + \int_{-\infty}^{w_{if}} \mathrm{e}^{\lambda_2(w_{if}-y)} g_{ie}(y)\mathrm{d}y \right) \\ \frac{-A_i}{h_i(0)} \left(\int_{w_{if}}^\infty \mathrm{e}^{\lambda_3(w_{if}-y)} g_{ii}(y)\mathrm{d}y + \int_{-\infty}^{w_{if}} \mathrm{e}^{\lambda_4(w_{if}-y)} g_{ii}(y)\mathrm{d}y \right) \end{pmatrix} \tag{14}$$

$$p_3(\lambda) = \begin{pmatrix} \frac{A_e}{h_e(w_{ef})} \left(\int_0^\infty \mathrm{e}^{\lambda_1(-y)} g_{ee}(y-w_{ef})\mathrm{d}y + \int_{-\infty}^0 \mathrm{e}^{\lambda_2(-y)} g_{ee}(y-w_{ef})\mathrm{d}y \right) \\ \frac{A_i}{h_e(w_{ef})} \left(\int_0^\infty \mathrm{e}^{\lambda_3(-y)} g_{ei}(y-w_{ef})\mathrm{d}y + \int_{-\infty}^0 \mathrm{e}^{\lambda_4(-y)} g_{ei}(y-w_{ef})\mathrm{d}y \right) \\ \frac{A_e}{h_e(w_{ef})} \left(\int_{wef}^\infty \mathrm{e}^{\lambda_1(w_{ef}-y)} g_{ee}(y-w_{ef})\mathrm{d}y + \int_{-\infty}^{w_{ef}} \mathrm{e}^{\lambda_2(w_{ef}-y)} g_{ee}(y-w_{ef})\mathrm{d}y \right) \\ \frac{A_i}{h_e(w_{ef})} \left(\int_{wef}^\infty \mathrm{e}^{\lambda_3(w_{ef}-y)} g_{ei}(y-w_{ef})\mathrm{d}y + \int_{-\infty}^{w_{ef}} \mathrm{e}^{\lambda_4(w_{ef}-y)} g_{ei}(y-w_{ef})\mathrm{d}y \right) \\ \frac{A_e}{h_e(w_{ef})} \left(\int_{w_{if}}^\infty \mathrm{e}^{\lambda_1(w_{if}-y)} g_{ee}(y-w_{ef})\mathrm{d}y + \int_{-\infty}^{w_{if}} \mathrm{e}^{\lambda_2(w_{if}-y)} g_{ee}(y-w_{ef})\mathrm{d}y \right) \\ \frac{A_i}{h_e(w_{ef})} \left(\int_{w_{if}}^\infty \mathrm{e}^{\lambda_3(w_{if}-y)} g_{ei}(y-w_{ef})\mathrm{d}y + \int_{-\infty}^{w_{if}} \mathrm{e}^{\lambda_4(w_{if}-y)} g_{ei}(y-w_{ef})\mathrm{d}y \right) \end{pmatrix} \tag{15}$$

$$p_6(\lambda) = \begin{pmatrix} \frac{-A_e}{h_i(w_{if})} \left(\int_0^\infty \mathrm{e}^{\lambda_1(-y)} g_{ie}(y-w_{if})\mathrm{d}y + \int_{-\infty}^0 \mathrm{e}^{\lambda_2(-y)} g_{ie}(y-w_{if})\mathrm{d}y \right) \\ \frac{-A_i}{h_i(w_{if})} \left(\int_0^\infty \mathrm{e}^{\lambda_3(-y)} g_{ii}(y-w_{if})\mathrm{d}y + \int_{-\infty}^0 \mathrm{e}^{\lambda_4(-y)} g_{ii}(y-w_{if})\mathrm{d}y \right) \\ \frac{-A_e}{h_i(w_{if})} \left(\int_{wef}^\infty \mathrm{e}^{\lambda_1(w_{ef}-y)} g_{ie}(y-w_{if})\mathrm{d}y + \int_{-\infty}^{w_{ef}} \mathrm{e}^{\lambda_2(w_{ef}-y)} g_{ie}(y-w_{if})\mathrm{d}y \right) \\ \frac{-A_i}{h_i(w_{if})} \left(\int_{wef}^\infty \mathrm{e}^{\lambda_3(w_{ef}-y)} g_{ii}(y-w_{if})\mathrm{d}y + \int_{-\infty}^{w_{ef}} \mathrm{e}^{\lambda_4(w_{ef}-y)} g_{ii}(y-w_{if})\mathrm{d}y \right) \\ \frac{-A_e}{h_i(w_{if})} \left(\int_{w_{if}}^\infty \mathrm{e}^{\lambda_1(w_{if}-y)} g_{ie}(y-w_{if})\mathrm{d}y + \int_{-\infty}^{w_{if}} \mathrm{e}^{\lambda_2(w_{if}-y)} g_{ie}(y-w_{if})\mathrm{d}y \right) \\ \frac{-A_i}{h_i(w_{if})} \left(\int_{w_{if}}^\infty \mathrm{e}^{\lambda_3(w_{if}-y)} g_{ii}(y-w_{if})\mathrm{d}y + \int_{-\infty}^{w_{if}} \mathrm{e}^{\lambda_4(w_{if}-y)} g_{ii}(y-w_{if})\mathrm{d}y \right) \end{pmatrix} \tag{16}$$

where $A_j = \frac{\alpha_j}{\sqrt{c^2+4D_j^2(\lambda+\alpha_j)}}$ for $j = \{e, i\}$. In Fig. 7, we classify the traveling wave solutions in the upper branches found in Fig. 4a as pulse (one-bump) or two-bump traveling wave solutions. As mentioned in the caption of Fig. 4, the parameters used in Figs. 4a, d and 7 show one of the best scenarios for existence of traveling waves in which the middle and upper branches that determine wave solutions lie in or very close to the range of interest. Using the Evans function, we determine the linear stability of the pulse solutions. We find that for values of D_i up to a point ($D_i \approx 140\,\mu\mathrm{m}/\sqrt{\mathrm{ms}}$ for the parameter choices in Fig. 7), the pulse solutions in the middle branch are linearly stable. Above that point, we have linearly unstable pulse solutions in the middle branch, which last up to the bifurcation value of D_i. The upper branch has two-bump solutions up to a point ($D_i \approx 185\,\mu\mathrm{m}/\sqrt{\mathrm{ms}}$) relatively close to the bifurcation value and unstable one-bump solutions above that point. The linear stability analysis also strengthens the discussion in Sect. 3 that a low or moderate gap junction coupling coefficient permits the existence of traveling wave solutions in the range of interest. In particular, to obtain linearly stable pulse solutions under the configuration of parameters determined by Fig. 7 with features very

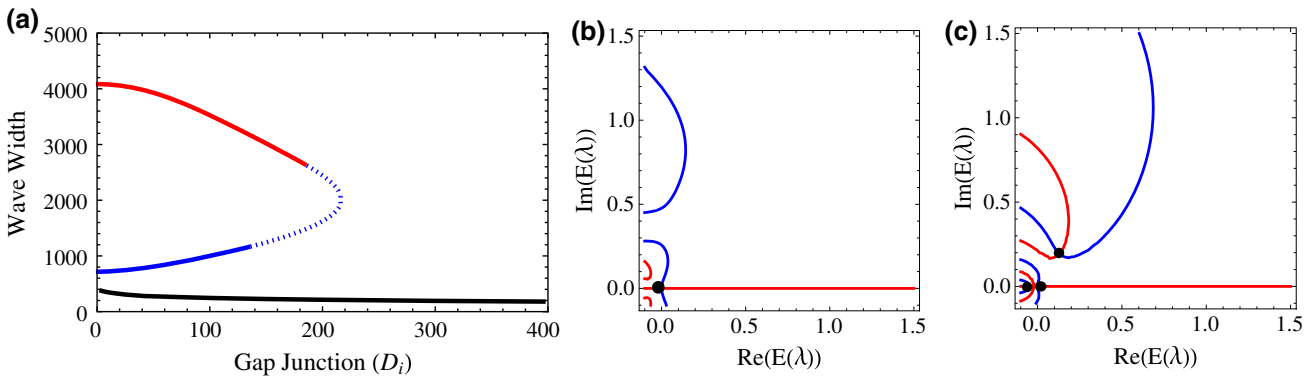

Fig. 7 Linear stability analysis of pulse solutions. **a** Stability analysis of Fig. 4a showing one-bump solutions (blue curves) and two-bump solutions (red curves). The linear stability analysis has been done for the one-bump solutions. The solid blue lines indicate linearly stable solutions (middle branch with $D_i \lesssim 140\,\mu\text{m}/\sqrt{\text{ms}}$) and the dashed blue lines indicate linearly unstable solutions (middle branch with $140 \lesssim D_i \lesssim 217\,\mu\text{m}/\sqrt{\text{ms}}$, and upper branch with $185 \lesssim D_i \lesssim 217\,\mu\text{m}/\sqrt{\text{ms}}$). The lower branch (black curve) is well below the range of interest, so it is not considered in this analysis. **b** Example of Evans function computation of a linearly stable solution. The graph shows the zero contour lines of the real part of the Evans function (red curve) and the imaginary part (blue curve). We observe only an intersection at the origin (black point) showing a simple zero eigenvalue due to the translationally invariant property of the wave solutions. **c** Example of Evans function computation of a linearly unstable solution. The eigenvalues are marked with black points. In addition to a simple zero eigenvalue, we observe an eigenvalue with negative real part and an eigenvalue with positive real part indicating wave instability. Parameters used for these plots: $\alpha_e = 1$ 1/ms, $\alpha_i = 0.1$ 1/ms, $\sigma_{ej} = 200$ and $\sigma_{ij} = 500$ for $j = \{e, i\}$, $D_e = \frac{D_i}{10}$. Wave solution features analyzed under the Evans function: **b** Linearly stable wave solution in the middle branch. $D_i = 1\,\mu\text{m}/\sqrt{\text{ms}}$, $c = 36\,\mu\text{m/ms}$ and $w = 716\,\mu\text{m}$. **c** Linearly unstable wave solution in the middle branch. $D_i = 200\,\mu\text{m}/\sqrt{\text{ms}}$, $c = 122\,\mu\text{m/ms}$ and $w = 1623\,\mu\text{m}$ (color figure online)

similar to in vivo clinical data, there is a limited range of values of D_i near $140\,\mu\text{m}/\sqrt{\text{ms}}$ (middle branch in Fig. 7a). If the diffusion coefficient is much less than $140\,\mu\text{m}/\sqrt{\text{ms}}$, then the features of the traveling wave solution are not as similar to in vivo waves. If the diffusion coefficient is more than $140\,\mu\text{m}/\sqrt{\text{ms}}$, then the traveling wave solution becomes linearly unstable, and after increasing the diffusion coefficient enough traveling wave solutions cease to exist. Thus, in this simple model, the effect of D_i is critical and we are able to replicate important features observed in vivo in a very limited range of values of the gap junction-like coefficient.

5 Numerical simulations

In this section, we corroborate our theoretical results by performing numerical simulations of model (1). The theoretical results in Fig. 4a, d show a bifurcation value of $D_i \approx 217\,\mu\text{m}/\sqrt{\text{ms}}$ above which traveling wave solutions no longer exist. Additionally, the linear stability analysis in Fig. 7 shows that the one-bump traveling wave solutions in the middle branch are stable for $D_i \lesssim 140\,\mu\text{m}/\sqrt{\text{ms}}$ and unstable for $140 \lesssim D_i \lesssim 217\,\mu\text{m}/\sqrt{\text{ms}}$. In the upper branch, one-bump solutions exist and are unstable for $185 \lesssim D_i \lesssim 217\,\mu\text{m}/\sqrt{\text{ms}}$. We therefore use numerical simulations to examine the behavior of the system (1) with values of D_i in each of these ranges.

Figure 8a shows the results of the numerical simulation with $D_i = 100\,\mu\text{m}/\sqrt{\text{ms}}$, in the linearly stable region of the middle branch. After a brief external input (in the form of a step function), the activity initially spreads outs and then converges on a traveling wave with a constant wave speed of $c \approx 65\,\mu\text{m/ms}$ and a constant wave width of $w \approx 990\,\mu\text{m}$. These values of c and w are similar to the analytic results in Fig. 4a, d.

The plots in Fig. 8c, d show the results of the numerical simulations with $D_i = 216\,\mu\text{m}/\sqrt{\text{ms}}$ corresponding to the middle and upper branches of Fig. 4a, d. Consistent with the instability demonstrated in Fig. 7, we were unable to find external inputs that led to traveling wave solutions with constant speed and width. We therefore initiated these simulations with the wave profiles determined from the analytic solutions. For a short amount of time, the wave propagates with speed and width similar to the values expected from the analytic results ($c \approx 140\,\mu\text{m}$ and $w \approx 1930\,\mu\text{m/ms}$ in Fig. 8c; $c \approx 148\,\mu\text{m/ms}$ and $w \approx 2080\,\mu\text{m}$ in Fig. 8d). After approximately 15 ms, the solution diverges noticeably from the traveling wave solution and no longer maintains constant speed and width. This behavior is consistent with the expected instability (Fig. 7) of the traveling wave solutions in this parameter range.

In Fig. 8b, we increase D_i to $218\,\mu\text{m}/\sqrt{\text{ms}}$, which is in the range above the bifurcation value where traveling wave solutions cease to exist. We observe that the width of the activity increases over time (from approximately $2090\,\mu\text{m}$ at $t = 0$ ms to approximately $2750\,\mu\text{m}$ at $t = 10$ ms). After $t \approx 10$ ms, the initial wave of activity splits into two waves whose widths then also spread out over time. Further increasing D_i

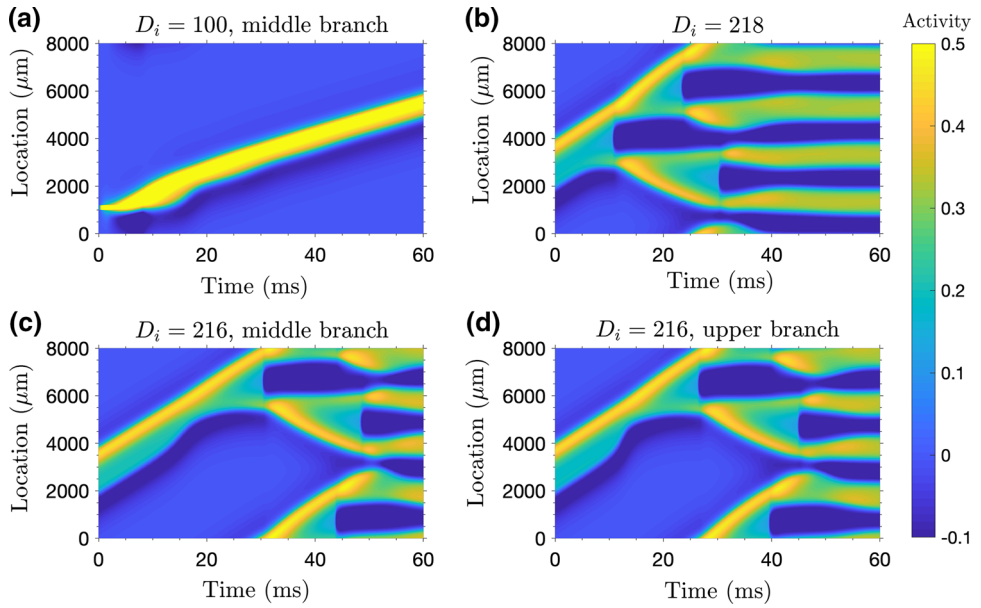

Fig. 8 Numerical simulations. We perform numerical simulations with various values of D_i above or below the bifurcation value ($D_i \approx 217\,\mu\text{m}/\sqrt{\text{ms}}$) identified in Fig. 4a, d. The plots in this figure show the activity (color scale) of the excitatory population as a function of space and time. **a** With $D_i = 100\,\mu\text{m}/\sqrt{\text{ms}}$, the numerical simulations support the existence and stability of a traveling wave solution corresponding to the middle branch of Figs. 4a, d and 7a. **b** When D_i is above the bifurcation value of $D_i \approx 217\,\mu\text{m}/\sqrt{\text{ms}}$, the wave spreads out over time, in contrast to traveling wave solutions where the width and speed remain constant over time. **c**, **d** With D_i slightly below the bifurcation value, simulations are shown corresponding to the middle (subplot **c**) and upper (subplot **d**) branches of Fig. 4a, d; the traveling wave solutions propagate for only a short amount of time before the wave width and wave speed diverge from constant values, supporting the conclusion in Fig. 7 that these traveling wave solutions are unstable. In all subplots, the numerical simulations were performed using Strang operator splitting with Euler's method for the nonlinear convolution terms and the Crank-Nicolson method for the decay and diffusion terms ($\Delta x = 1\,\mu\text{m}$, $\Delta t = 0.005$ ms, and the spatial domain has periodic boundary conditions). For **a**, a brief step-function input was used to initiate activity. For **c**, **d**, we consider initial conditions determined by the profiles expected from the analytic solution (3) and (4). For **b**, no analytic solution exists in the range of interest, so the initial conditions and thresholds from **d** were used. Parameters fixed in all subplots: $\alpha_e = 1$ 1/ms, $\alpha_i = 0.1$ 1/ms, $\sigma_{ej} = 200\,\mu\text{m}$ and $\sigma_{ij} = 500\,\mu\text{m}$ for $j = \{e, i\}$, $D_e = \frac{D_i}{10}$. Parameters that differ by subplot: **a** $D_i = 100\,\mu\text{m}/\sqrt{\text{ms}}$, $k_e = 0.235001$, $k_i = 0.273941$; **b** $D_i = 218\,\mu\text{m}/\sqrt{\text{ms}}$, $k_e = 0.121415$, $k_i = 0.126148$; **c** $D_i = 216\,\mu\text{m}/\sqrt{\text{ms}}$, $k_e = 0.127676$, $k_i = 0.132995$; **d** $D_i = 216\,\mu\text{m}/\sqrt{\text{ms}}$, $k_e = 0.121415$, $k_i = 0.126148$

produces results that are qualitatively similar to Fig. 8b, but the wave spreads out faster and splits in two earlier as D_i increases. Thus, the numerical results shown in Fig. 8 support our theoretical analysis.

6 Conclusions

In this paper, we investigate the possible effect of gap junctions on seizure wave propagation preceding seizure termination. Using a voltage-based neural field model including gap junctions, we are able to replicate traveling wave solutions with features observed in vivo. In our analysis, we find the existence of a critical value of the gap junction connectivity such that one-bump and two-bump traveling wave solutions with the desired speed and width cease to exist. Above this critical value, wave solutions tend to spread out over time due to the effect of gap junction connectivity. Both one-bump and two-bump solutions successfully reproduce wave features observed in vivo. Two-bump solutions could help to replicate the reverberation of activity that has been observed in seizure wave propagation preceding seizure termination. Stability analysis performed in this model suggests that there is a critical value of the gap junction-like coefficient that permits the existence of one-bump linearly stable solutions with features similar to the observed waves. Therefore, these results provide support to existing evidence found in the literature suggesting a key role of gap junctions during seizure wave propagation. However, it is important to note that this is a simple model that produces traveling wave behavior of interest. Future extensions for developing more biophysically realistic models could include the incorporation of the dynamic nature of gap junctions or their aggregation, as well as a key factor concerning the difference between the timescales of action of chemical and electrical synapses. It is necessary to establish more realistic biophysical models to study the exact role of gap junctions during epileptic seizures.

A Appendix: Model motivation

A biophysically based and widely used model for describing the somatic membrane potential $V_i(t)$ of a single neuron is Ermentrout (1998); Bressloff (2012):

$$C\frac{\mathrm{d}V_i}{\mathrm{d}t} = -I_{\mathrm{con}} + I_{\mathrm{syn}} + I_{\mathrm{gap}} + I_{\mathrm{ext}} \tag{17}$$

where C is the cell capacitance, I_{con} is the membrane current, I_{syn} denotes the (chemical) synaptic input currents entering the cell, I_{gap} denotes gap junction input currents and I_{ext} are any external currents. For the moment, we ignore the external currents.

The membrane current is modeled by Ohm's Law and determined by the term $I_{\mathrm{con}}=\sum_k g_k(V - E_k)$, where each k determines a specific ion diffusing through channels in the cell membrane, and g_k and E_k determine the gating dynamics and reversal potential of the kth channel, respectively.

We assume that the net chemical synaptic input into neuron i from a population of neurons is determined by $I_{\mathrm{syn}} = \sum_j \sum_m g_j(t - T_j^m)(V_{\mathrm{syn}} - V(t))$, where g_j represents the synaptic dynamics determined by presynaptic neuron j, V_{syn} is the synaptic reversal potential, and T_j^m determines a distribution of firing times of neuron j. Here, we consider no synaptic depression and ignore dendritic architecture. Also, we assume that the chemical synaptic inputs sum linearly.

Gap junctions allow direct diffusion of ions and small molecules between adjacent cells (Goodenough and Paul 2009). Therefore, we assume that the gap junctions are also modeled by Ohm's Law in a diffusive manner $I_{\mathrm{gap}} = \sum_j \frac{1}{R}(V_j - V_i)$ where R is the resistance.

Therefore, we obtain from (17):

$$\begin{aligned} C\frac{\mathrm{d}V_i}{\mathrm{d}t} = &-I_{\mathrm{con}} + \sum_j \sum_m g_j(t - T_j^m)(V_{\mathrm{syn}} - V(t)) \\ &+ \sum_j \frac{1}{R}(V_j - V_i) \end{aligned} \tag{18}$$

We observe that the term I_{gap} resembles the discretization of a one-dimensional second spatial derivative (similar to Steyn-Ross et al. 2007). That is, considering three aligned neurons $j-1$, j and $j+1$, the input from gap junction coupling on cell j is

$$\begin{aligned} &\frac{1}{R}\left(\left(V_{j-1} - V_j\right) + \left(V_{j+1} - V_j\right)\right) \\ &= \frac{1}{R}\left(V_{j-1} - 2V_j + V_{j+1}\right) \\ &= \frac{(\Delta x)^2}{R}\frac{\left(V_{j-1} - 2V_j + V_{j+1}\right)}{(\Delta x)^2} \\ &\approx D_j^2 \frac{\partial^2 V_j}{\partial x^2} \end{aligned} \tag{19}$$

Without the inclusion of gap junctions, (18) can be further reduced. This is done by considering a temporal averaging of (18) to obtain a closed system of integral equations to later reduce to Wilson–Cowan or Amari-type equations (Ermentrout 1998; Bressloff 2012). The potential V_i can be considered to be converted into a firing rate by means of a nonlinear function. This can help to establish the potential in a network of neurons as a set of Volterra equations that can be further reduced into the voltage-based model (20). In this reduction, the variable u_e now accounts for a mean variable denoting the activity of a neuronal population. We note that model (20) does not include action potentials. For this reduction to happen, it is necessary to include the assumption of a slowly acting synaptic current. However, we have mentioned that gap junctions are faster-acting than chemical synaptic current, so this assumption is not valid for gap junctions. We suggest that this may be rectified by considering instead an anomalous diffusion. As a step in this direction, we propose a simple model considering an excitatory and inhibitory population, together with both chemical and electrical synapses, where the electrical synapses are modeled by simple diffusion:

$$\begin{aligned} \frac{\partial u_e}{\partial t}(x,t) = &-\alpha_e u_e(x,t) + \alpha_e g_{ee} \otimes H(u_e(x,t) - k_e) \\ &- \alpha_e g_{ie} \otimes H(u_i(x,t) - k_i) + D_{\mathrm{e}}^2 \frac{\partial^2 u_e}{\partial x^2}(x,t) \\ \frac{\partial u_i}{\partial t}(x,t) = &-\alpha_i u_i(x,t) + \alpha_i g_{ei} \otimes H(u_e(x,t) - k_e) \\ &- \alpha_i g_{ii} \otimes H(u_i(x,t) - k_i) + D_i^2 \frac{\partial^2 u_i}{\partial x^2}(x,t) \end{aligned} \tag{20}$$

In this model, there is no dynamic component for the gap junction coupling and architecture of the gap junction distribution is not considered. However, we propose that this model is of interest for determining if wave propagation as observed in vivo preceding seizure termination is possible under a simple scenario. This could provide a useful foundation for developing more realistic models including gap junction coupling that mimic wave features observed in vivo.

B Appendix: Traveling wave solutions

We now provide a sketch of the derivation of the traveling wave solutions (3) and (4). We first consider system (1) in moving frame (z,t) where $z = x - ct$. We look for stationary solutions of this system such that $\frac{\partial u_j}{\partial t}(z,t) = 0$, implying $u_j(z,t) = u_j(z)$ where $j = \{e,i\}$. We derive a Green's function (Stakgold and Holst 2011; Evans 2010) that helps solve the inhomogeneous differential system that arises. The Green's function that we derive has the following form:

$$G(z,s)=\begin{cases}\frac{\alpha_j}{\sqrt{c^2+4\alpha_j D_j^2}}\exp\left(r_1\left(z-s\right)\right) & \text{if } z\le s\\ \frac{\alpha_j}{\sqrt{c^2+4\alpha_j D_j^2}}\exp\left(r_2\left(z-s\right)\right) & \text{if } s<z\end{cases} \tag{21}$$

where $r_1=\frac{-c+\sqrt{c^2+4\alpha_j D_j^2}}{2D_j^2}$, and $r_2=\frac{-c-\sqrt{c^2+4\alpha_j D_j^2}}{2D_j^2}$. This Green's function solves the inhomogeneous system by considering:

$$u_j(z)=\int_{-\infty}^{\infty}G(z,s)P(s)\mathrm{d}y \tag{22}$$

$$\begin{aligned}P(s)=&\int_{-\infty}^{\infty}g_{ej}(s-y)H(u_e(y)-k_e)\\&-g_{ij}(s-y)H(u_i(y)-k_i)\mathrm{d}y\end{aligned} \tag{23}$$

where $g_{jk}=\frac{1}{2\sigma_{jk}}\exp\left(-\frac{|x|}{\sigma_{jk}}\right)$ and H is the Heaviside function. Assuming $u_j(y)>k_j$ for $w_{j0}<y<w_{jf}$ we obtain:

$$P(s)=\int_{s-w_{ef}}^{s-we0}g_{ej}(y)\mathrm{d}y-\int_{s-wif}^{s-wi0}g_{ij}(y)\mathrm{d}y \tag{24}$$

Assuming $w_{i0}\le w_{e0}\le w_{if}\le w_{ef}$ and substituting (21) and (24) into (22) we obtain the traveling wave solutions (3) and (4):

$$u_j^{\star}(z)=\begin{cases}u_{j1} & \text{if } z\le w_{i0}\\ u_{j2} & \text{if } w_{i0}<z\le w_{e0}\\ u_{j3} & \text{if } w_{e0}<z\le w_{if}\\ u_{j4} & \text{if } w_{if}<z\le w_{ef}\\ u_{j5} & \text{if } z>w_{ef}\end{cases} \tag{25}$$

where

$$\begin{aligned}u_{j1}(z)=&\left(\frac{\alpha_j}{2\sqrt{c^2+4\alpha_j D_j^2}}\right)\Bigg[\exp\left(\frac{z-w_{e0}}{\sigma_{ej}}\right)\\&\times\left(\frac{\sigma_{ej}}{1-\sigma_{ej}r_2}-\frac{\sigma_{ej}}{1-\sigma_{ej}r_1}\right)\\&+\exp\left(\frac{z-w_{ef}}{\sigma_{ej}}\right)\left(\frac{\sigma_{ej}}{1-\sigma_{ej}r_1}-\frac{\sigma_{ej}}{1-\sigma_{ej}r_2}\right)\\&+\exp\left(\frac{z-w_{if}}{\sigma_{ij}}\right)\left(\frac{\sigma_{ij}}{1-\sigma_{ij}r_2}-\frac{\sigma_{ij}}{1-\sigma_{ij}r_1}\right)\\&+\exp(\frac{z-w_{i0}}{\sigma_{ij}})\left(\frac{\sigma_{ij}}{1-\sigma_{ij}r_1}-\frac{\sigma_{ij}}{1-\sigma_{ij}r_2}\right)\\&+\exp\left(r_1(z-w_{e0})\right)\left(\frac{\sigma_{ej}}{1-\sigma_{ej}r_1}-\frac{\sigma_{ej}}{1+\sigma_{ej}r_1}+\frac{2}{r_1}\right)\\&+\exp\left(r_1(z-w_{ef})\right)\left(\frac{\sigma_{ej}}{1+\sigma_{ej}r_1}-\frac{\sigma_{ej}}{1-\sigma_{ej}r_1}-\frac{2}{r_1}\right)\\&+\exp\left(r_1(z-w_{i0})\right)\left(\frac{\sigma_{ij}}{1+\sigma_{ij}r_1}-\frac{\sigma_{ij}}{1-\sigma_{ij}r_1}-\frac{2}{r_1}\right)\\&+\exp\left(r_1(z-w_{if})\right)\left(\frac{\sigma_{ij}}{1-\sigma_{ij}r_1}-\frac{\sigma_{ij}}{1+\sigma_{ij}r_1}+\frac{2}{r_1}\right)\Bigg]\end{aligned} \tag{26}$$

$$\begin{aligned}u_{j2}(z)=&\left(\frac{\alpha_j}{2\sqrt{c^2+4\alpha_j D_j^2}}\right)\Bigg[\exp\left(\frac{z-w_{e0}}{\sigma_{ej}}\right)\\&\times\left(\frac{\sigma_{ej}}{1-\sigma_{ej}r_2}-\frac{\sigma_{ej}}{1-\sigma_{ej}r_1}\right)\\&+\exp\left(\frac{z-w_{ef}}{\sigma_{ej}}\right)\left(\frac{\sigma_{ej}}{1-\sigma_{ej}r_1}-\frac{\sigma_{ej}}{1-\sigma_{ej}r_2}\right)\\&+\exp\left(\frac{z-w_{if}}{\sigma_{ij}}\right)\left(\frac{\sigma_{ij}}{1-\sigma_{ij}r_2}-\frac{\sigma_{ij}}{1-\sigma_{ij}r_1}\right)\\&+\exp(\frac{-(z-w_{i0})}{\sigma_{ij}})\left(\frac{\sigma_{ij}}{1+\sigma_{ij}r_1}-\frac{\sigma_{ij}}{1+\sigma_{ij}r_2}\right)\\&+\exp\left(r_1(z-w_{e0})\right)\left(\frac{\sigma_{ej}}{1-\sigma_{ej}r_1}-\frac{\sigma_{ej}}{1+\sigma_{ej}r_1}+\frac{2}{r_1}\right)\\&+\exp\left(r_1(z-w_{ef})\right)\left(\frac{\sigma_{ej}}{1+\sigma_{ej}r_1}-\frac{\sigma_{ej}}{1-\sigma_{ej}r_1}-\frac{2}{r_1}\right)\\&+\exp\left(r_2(z-w_{i0})\right)\left(\frac{\sigma_{ij}}{1+\sigma_{ij}r_2}-\frac{\sigma_{ij}}{1-\sigma_{ij}r_2}-\frac{2}{r_2}\right)\\&+\exp\left(r_1(z-w_{if})\right)\left(\frac{\sigma_{ij}}{1-\sigma_{ij}r_1}-\frac{\sigma_{ij}}{1+\sigma_{ij}r_1}+\frac{2}{r_1}\right)\\&+\left(\frac{2}{r_2}-\frac{2}{r_1}\right)\Bigg]\end{aligned}$$

$$\begin{aligned}u_{j3}(z)=&\left(\frac{\alpha_j}{2\sqrt{c^2+4\alpha_j D_j^2}}\right)\Bigg[\exp\left(\frac{-(z-w_{e0})}{\sigma_{ej}}\right)\\&\times\left(\frac{\sigma_{ej}}{1+\sigma_{ej}r_2}-\frac{\sigma_{ej}}{1+\sigma_{ej}r_1}\right)\\&+\exp\left(\frac{z-w_{ef}}{\sigma_{ej}}\right)\left(\frac{\sigma_{ej}}{1-\sigma_{ej}r_1}-\frac{\sigma_{ej}}{1-\sigma_{ej}r_2}\right)\\&+\exp\left(\frac{z-w_{if}}{\sigma_{ij}}\right)\left(\frac{\sigma_{ij}}{1-\sigma_{ij}r_2}-\frac{\sigma_{ij}}{1-\sigma_{ij}r_1}\right)\\&+\exp(\frac{-(z-w_{i0})}{\sigma_{ij}})\left(\frac{\sigma_{ij}}{1+\sigma_{ij}r_1}-\frac{\sigma_{ij}}{1+\sigma_{ij}r_2}\right)\\&+\exp\left(r_2(z-w_{e0})\right)\left(\frac{\sigma_{ej}}{1-\sigma_{ej}r_2}-\frac{\sigma_{ej}}{1+\sigma_{ej}r_2}+\frac{2}{r_2}\right)\\&+\exp\left(r_1(z-w_{ef})\right)\left(\frac{\sigma_{ej}}{1+\sigma_{ej}r_1}-\frac{\sigma_{ej}}{1-\sigma_{ej}r_1}-\frac{2}{r_1}\right)\\&+\exp\left(r_2(z-w_{i0})\right)\left(\frac{\sigma_{ij}}{1+\sigma_{ij}r_2}-\frac{\sigma_{ij}}{1-\sigma_{ij}r_2}-\frac{2}{r_2}\right)\\&+\exp\left(r_1(z-w_{if})\right)\left(\frac{\sigma_{ij}}{1-\sigma_{ij}r_1}-\frac{\sigma_{ij}}{1+\sigma_{ij}r_1}+\frac{2}{r_1}\right)\Bigg]\end{aligned} \tag{27}$$

$$\begin{aligned}u_{j4}(z)=&\left(\frac{\alpha_j}{2\sqrt{c^2+4\alpha_j D_j^2}}\right)\Bigg[\exp\left(\frac{-(z-w_{e0})}{\sigma_{ej}}\right)\\&\times\left(\frac{\sigma_{ej}}{1+\sigma_{ej}r_2}-\frac{\sigma_{ej}}{1+\sigma_{ej}r_1}\right)\\&+\exp\left(\frac{z-w_{ef}}{\sigma_{ej}}\right)\left(\frac{\sigma_{ej}}{1-\sigma_{ej}r_1}-\frac{\sigma_{ej}}{1-\sigma_{ej}r_2}\right)\\&+\exp\left(\frac{-(z-w_{if})}{\sigma_{ij}}\right)\left(\frac{\sigma_{ij}}{1+\sigma_{ij}r_2}-\frac{\sigma_{ij}}{1+\sigma_{ij}r_1}\right)\end{aligned}$$

$$+\exp(\frac{-(z-w_{i0})}{\sigma_{ij}})\left(\frac{\sigma_{ij}}{1+\sigma_{ij}r_1}-\frac{\sigma_{ij}}{1+\sigma_{ij}r_2}\right)$$
$$+\exp\left(r_2(z-w_{e0})\right)\left(\frac{\sigma_{ej}}{1-\sigma_{ej}r_2}-\frac{\sigma_{ej}}{1+\sigma_{ej}r_2}+\frac{2}{r_2}\right)$$
$$+\exp\left(r_1(z-w_{ef})\right)\left(\frac{\sigma_{ej}}{1+\sigma_{ej}r_1}-\frac{\sigma_{ej}}{1-\sigma_{ej}r_1}-\frac{2}{r_1}\right)$$
$$+\exp\left(r_2(z-w_{i0})\right)\left(\frac{\sigma_{ij}}{1+\sigma_{ij}r_2}-\frac{\sigma_{ij}}{1-\sigma_{ij}r_2}-\frac{2}{r_2}\right)$$
$$+\exp\left(r_2(z-w_{if})\right)\left(\frac{\sigma_{ij}}{1-\sigma_{ij}r_2}-\frac{\sigma_{ij}}{1+\sigma_{ij}r_2}+\frac{2}{r_2}\right)$$
$$+\left(\frac{2}{r_1}-\frac{2}{r_2}\right)\Bigg] \tag{28}$$

$$u_{j5}(z)=\left(\frac{\alpha_j}{2\sqrt{c^2+4\alpha_j D_j^2}}\right)\Bigg[\exp\left(\frac{-(z-w_{e0})}{\sigma_{ej}}\right)$$
$$\times\left(\frac{\sigma_{ej}}{1+\sigma_{ej}r_2}-\frac{\sigma_{ej}}{1+\sigma_{ej}r_1}\right)$$
$$+\exp\left(\frac{-(z-w_{ef})}{\sigma_{ej}}\right)\left(\frac{\sigma_{ej}}{1+\sigma_{ej}r_1}-\frac{\sigma_{ej}}{1+\sigma_{ej}r_2}\right)$$
$$+\exp\left(\frac{-(z-w_{if})}{\sigma_{ij}}\right)\left(\frac{\sigma_{ij}}{1+\sigma_{ij}r_2}-\frac{\sigma_{ij}}{1+\sigma_{ij}r_1}\right)$$
$$+\exp(\frac{-(z-w_{i0})}{\sigma_{ij}})\left(\frac{\sigma_{ij}}{1+\sigma_{ij}r_1}-\frac{\sigma_{ij}}{1+\sigma_{ij}r_2}\right)$$
$$+\exp\left(r_2(z-w_{e0})\right)\left(\frac{\sigma_{ej}}{1-\sigma_{ej}r_2}-\frac{\sigma_{ej}}{1+\sigma_{ej}r_2}+\frac{2}{r_2}\right)$$
$$+\exp\left(r_2(z-w_{ef})\right)\left(\frac{\sigma_{ej}}{1+\sigma_{ej}r_2}-\frac{\sigma_{ej}}{1-\sigma_{ej}r_2}-\frac{2}{r_2}\right)$$
$$+\exp\left(r_2(z-w_{i0})\right)\left(\frac{\sigma_{ij}}{1+\sigma_{ij}r_2}-\frac{\sigma_{ij}}{1-\sigma_{ij}r_2}-\frac{2}{r_2}\right)$$
$$+\exp\left(r_2(z-w_{if})\right)\left(\frac{\sigma_{ij}}{1-\sigma_{ij}r_2}-\frac{\sigma_{ij}}{1+\sigma_{ij}r_2}+\frac{2}{r_2}\right)\Bigg] \tag{29}$$

References

Amari S (1977) Dynamics of pattern formation in lateral-inhibition type neural fields. Biol Cybern 27:77–87

Braitenberg V, Schuz A (1998) Cortex: statistics and geometry of neuronal connectivity. Springer, Berlin

Bressloff P (2012) Spatiotemporal dynamics of continuum neural fields. J Phys A Math Theor 45(3):033001

Bressloff P (2016) Diffusion in cells with stochastically gated gap junctions. SIAM J Appl Math 76:1658–1682

Bressloff P, Cowan J, Golubitsky M, Thomas P, Wiener M (2001) Geometric visual hallucinations, euclidean symmetry and the functional architecture of striate cortex. Philos Trans R Soc B 356:299–330

Carlen P, Skinner F, Zhang L, Naus C, Kushnir ea M (2000) The role of gap junctions in seizures. Brain Res Rev 32:235–241

Chen L, Meng M (1995) Compact and scattered gap junctions in diffusion mediated cell–cell communication. J Theor Biol 176:39–45

Chow C, Kopell N (2000) Dynamics of spiking neurons with electrical coupling. Neural Comput 12:1643–1678

Coombes S (2005) Waves, bumps, and patterns in neural field theories. Biol Cybern 93:91–108

Coombes S (2008) Neuronal networks with gap junctions: a study of piecewise linear planar neuron models. SIAM J Appl Dyn Syst 7:1101–1129

Coombes S, Zachariou M (2009) Gap junctions and emergent rhythms. In: Josic K, Rubin J, Matias M, Romo R (eds) Coherent behavior in neuronal networks. Springer series in computational neuroscience, vol 3. Springer, New York, NY

Coombes S, Beim Graben P, Potthast R, Wright J (2014) Neural fields: theory and applications. Springer, Berlin

Dudek F, Yasamura T, JE R (1998) Non-synaptic mechanisms in seizures and epileptogenesis. Cell Biol Int 22:793–805

Elvin A (2008) Pattern formation in a neural field model. PhD thesis, Massey University, College of Sciences

Ermentrout G (1998) Neural networks as spatio-temporal pattern-forming systems. Rep Prog Phys 61:353–430

Ermentrout G (2006) Gap junctions destroy persistent states in excitatory networks. Phys Rev E Stat Nonlinear Soft Matter Phys 74:031918

Ermentrout G, Cowan J (1979) A mathematical theory of visual hallucination patterns. Biol Cybern 34:137–150

Ermentrout G, Terman D (2010) Mathematical foundations of neuroscience. Springer, Berlin

Evangelista E, Benar C, Bonini F, Carron R, Colombet B, Regis J, Bartolomei F (2015) Does the thalamo-cortical synchrony play a role in seizure termination? Front Neurol 6:192

Evans L (2010) Partial differential equations, 2nd edn. American Mathematical Society, Providence

Evans W, Martin P (2002) Gap junctions: structure and function. Mol Membr Biol 19:121–136

Foster B, Boja I, Liley D (2011) Understanding the effects of anesthetic agents on the EEG through neural field theory. In: Conference proceedings of IEEE engineering in medicine and biology society, vol 652

Frascoli F, Van Veen L, Bojak I, Liley D (2011) Metabifurcation analysis of a mean field model of the cortex. Physica D 240:949–962

Fujii Y, Maekawa S, Morita M (2017) Astrocyte calcium waves propagate proximally by gap junction and distally by extracellular diffusion of ATP released from volume-regulated anion channels. Sci Rep 7:13115

Fukuda T, Kosaka T, Singer W, Galuske R (2006) Gap junctions among dendrites of cortical gabaergic neurons establish a dense and widespread intercolumnar network. J Neurosci 26(13):3434–3443

González-Ramírez L, Kramer M (2018) The effect of inhibition on the existence of traveling wave solutions for a neural field model of human seizure termination. J Comput Neurosci 44(3):393–409

González-Ramírez L, Ahmed O, Cash S, Wayne C, Kramer M (2015) A biologically constrained, mathematical model of cortical wave propagation preceding seizure termination. PLoS Comput Biol 11:e1004065

Goodenough D, Paul D (2009) Gap junctions. Cold Spring Harb Perspect Biol 1:a002576

Jin M, Chen Z (2011) Role of gap junctions in epilepsy. Neurosci Bull 27(6):389–406

Jirsa VK, Stacey WC, Quilichini PP, Ivanov I, Bernard C (2014) On the nature of seizure dynamics. Brain 137:2210–2230

Kapitula T, Kutz N, Sandstede B (2004) The evans function for nonlocal equations. Indiana Univ Math J 53:1095–1126

Keener J, Sneyd J (1998) Mathematical physiology. Springer, New York

Kepler T, Marder E, Abbott L (1990) The effect of electrical coupling on the frequency of model neuronal oscillators. Science 248:83–85

Kopell N, Ermentrout B (2004) Chemical and electrical synapses perform complementary roles in the synchronization of interneuronal networks. Proc Natl Acad Sci USA 101:15482–15487

Lacar B, Young S, Platel J, Bordey A (2011) Gap junction-mediated calcium waves define communication networks among murine

postnatal neural progenitor cells. Eur J Neurosci 34(12):1895–1905
Laing C (2015) Exact neural fields incorporating gap junctions. SIAM J Appl Dyn Syst 14(4):1899–1929
Lewis T, Rinzel J (2003) Dynamics of spiking neurons connected by both inhibitory and electrical coupling. J Comput Neurosci 14:283–309
Liley D, Cadusch P, Dafilis M (2002) A spatially continuous mean field theory of electrocortical activity. Network 13:67–113
Martinet LE, Fiddyment G, Madsen JR, Eskandar EN, Truccolo W, Eden UT, Cash SS, Kramer MA (2017) Human seizures couple across spatial scales through travelling wave dynamics. Nat Commun 8:14896
Mylvaganam S, Ramani M, Krawczyk M, Carlen P (2014) Roles of gap junctions, connexins, and pannexins in epilepsy. Front Physiol 5:172
Perucca P, Dubeau F, Gotman J (2013) Intracranial electroencephalographic seizure-onset patterns: effect of underlying pathology. Brain 137:183–96
Peyrache A, Dehghani N, Eskandar E et al (2012) Spatiotemporal dynamics of neocortical excitation and inhibition during human sleep. PNAS 109(5):1731–1736
Proix T, Jirsa VK, Bartolomei F, Guye M, Wilson T (2018) Predicting the spatiotemporal diversity of seizure propagation and termination in human focal epilepsy. Nat Commun 9:1088
Reimann M, Anastassiou C, Perin R, Hill S, Markram H et al (2013) A biophysically detailed model of neocortical local field potentials predicts the critical role of active membrane currents. Neuron 79:375–390
Rose B, Loewenstein W (1976) Permeability of a cell junction and the local cytoplasmic free ionised calcium concentration; a study with aequorin. J Membr Biol 28:87–119
Saez J, Connor J, Spray D, Bennett M (1989) Hepatocyte gap junctions are permeable to the second messenger, inositol 1,4,5-trisphosphate, and to calcium ions. Proc Natl Acad Sci USA 86:2708–2712
Sandstede B (2002) Stability of travelling waves. Handb Dyn Syst 2:983–1055
Sandstede B (2007) Evans function and nonlinear stability of traveling waves in neuronal network models. Int J Bifurc Chaos 17:2693–2704
Schevon CA, Weiss SA, McKhann G, Goodman RR, Yuste R, Emerson RG, Trevelyan AJ (2012) Evidence of an inhibitory restraint of seizure activity in humans. Nat Commun 3:1060
Schmitz D, Schuchmann S, Fisahn A, Draguhn A, Buhl E et al (2001) Axo-axonal coupling: a novel mechanism for ultrafast neuronal communication. Neuron 31(5):831–840
Sherman A, Rinzel J (1992) Rhythmogenic effects of weak electrotonic coupling in neuronal models. Proc Nat Acad Sci USA 89:2471–2474
Smith EH, Liou JY, Davis TS, Merricks EM, Kellis SS, Weiss SA, Greger B, House PA, McKhann GM, Goofman RR, Emerson RG, Bateman LM, Trevelyan AJ, Schevon CA (2016) The ictal wavefront is the spatiotemporal source of discharges during spontaneous human seizures. Nat Commun 7:11098
Stakgold I, Holst M (2011) Green's functions and boundary value problems, 3rd edn. Wiley, New Jersey
Steyn-Ross M, Steyn-Ross D, Wilson M, Sleigh JW (2007) Gap junctions mediate large-scale turing structures in a mean-field cortex driven by subcortical noise. Phys Rev E 76:011916
Steyn-Ross M, Steyn-Ross D, Sleigh JW (2012) Gap junctions modulate seizures in a mean field-model of general anesthesia for the cortex. Cogn Neurodyn 6:215–225
Weiss SA, Banks GP, McKhann GMJ, Goodman RR, Emerson RG, Trevelyan AJ, Schevon C (2013) Ictal high frequency oscillations distinguish two types of seizure territories in humans. Brain 136:3796–808
Wilson H, Cowan J (1972) Excitatory and inhibitory interactions in localized populations of model neurons. Biophys J 12:1–24
Zhang M, Ladas T, Qiu C, Shivacharan R, Gonzalez-Reyes L, Durand D (2014) Propagation of epileptiform activity can be independent of synaptic transmission, gap junctions, or diffusion and is consistent with electrical field transmission. J Neurosci 34(4):1409–1419
Zhao X, Robinson P (2015) Generalized seizures in a neural field model with bursting dynamics. J Comput Neurosci 39:197–216